Single-Crystal Sapphire Optical Fiber Sensor Instrumentation

Final Report

DOE Award Number: DE-FC26-99FT40685

Reporting Period Start Date: 01 October 1999
Reporting Period End Date: 30 June 2002

Issue Date: 18 October 2002

Principal Authors: A. Wang, G. Pickrell, and R. May

Submitted by: Center for Photonics Technology
Bradley Department of Electrical and Computer Engineering
Virginia Tech
Blacksburg, VA 24061-0111

CPT

CENTER FOR PHOTONICS TECHNOLOGY

Disclaimer

Abstract

Accurate measurement of temperature is essential for the safe and efficient operation and control of a wide range of industrial processes. Appropriate techniques and instrumentation are needed depending on the temperature measurement requirements in different industrial processes and working environments. Harsh environments are common in many industrial applications. These harsh environments may involve extreme physical conditions, such as high-temperature, high-pressure, corrosive agents, toxicity, strong electromagnetic interference, and high-energy radiation exposure. Due to these severe environmental conditions, conventional temperature sensors are often difficult to apply. This situation has opened a new but challenging opportunity for the sensor society to provide robust, high-performance, and cost-effective temperature sensors capable of operating in those harsh environments.

The focus of this research program has been to develop a temperature measurement system for temperature measurements in the primary and secondary stages of slagging gasifiers. For this application the temperature measurement system must be able to withstand the extremely harsh environment posed by the high temperatures and corrosive agents present in these systems. Real-time, accurate and reliable monitoring of temperature for the coal gasification process is important to realize the full economic potential of these gasification systems. Long life and stability of operation in the high temperature environment is essential for the temperature measurement system to ensure the continuous running of the coal gasification system over the long term. In this high

temperature and chemically corrosive environment, rather limited high temperature measurement techniques such as high temperature thermocouples and optical /acoustic pyrometers are available, each with their own limitations.

In this research program, five different temperature sensing schemes based on the single crystal sapphire material were thoroughly investigated to determine an optimal approach for on-line, real-time, reliable, long-term monitoring of temperatures inside the coal gasification environment. Among these were a sapphire fiber extrinsic Fabry-Pérot interferometric (EFPI) sensor; an intensity-measurement based polarimetric sapphire sensor and a broadband polarimetric differential interferometric (BPDI) sapphire sensor. Based on the current evaluation and analysis of the experimental results, the broadband polarimetric differential interferometric (BPDI) sensor system was chosen for further prototype instrumentation development because of it's superior performance compared to the other systems. This approach is based on the self-calibrating measurement of the optical path length differences in a single-crystal sapphire disk, which is a function of both the temperature dependent birefringence and the temperature dependent dimensional changes.

In the BPDI system, a spectrometer is incorporated with a polarimeter for the purpose of measuring polarization properties as a function of wavelength. It offers the following major advantages over other designed sensors:

1. The BPDI technology extracts absolute temperature information by absolute measurement of phase delays, which are much more suitable in applications for

harsh environments because of the lack ofinitialization and/or calibration when the power is switched on.

2. The BPDI optical temperature measurement system takes advantages of both optical fibers and bulk optics to simplify the sensing head design. Bulk optics is convenient for reducing the required tolerances on optical alignment and also for reducing the sensitivity to vibration. The optical fiber can transmit light for a long distance with small attenuation and be easily implemented in industrial environments because of its small size, lightweight and immunity to electromagnetic interference (EMI).

3. Since the BPDI sensor system measures the interference caused by the phase delay of two orthogonally polarized light waves, it offers high measurement resolution because of theintrinsic interferometric character of the sensor.

4. The BPDI system monitors real-time temperatures through measurement of the relative spectral shift of adjacent peaks in the interference spectrum instead of the optical intensity. Since the system is wavelength based (not intensity based)it is immune to optical source power fluctuations and fiber losses, thus providing a relatively high degree of long-term measurement stability.

Table of Contents

List of Figures

3

4

Chapter 1. Introduction

Temperature is the most common measurement in industrial process applications since the rate of every process, in nature and in industry, is temperature dependent. The accurate measurement of temperature is essential for the safe and efficient operation and control of a vast range of industrial processes. Appropriate techniques and instrumentation are needed depending on the temperature measurement requirements in different industrial processes and working environments.

Harsh environments are often unavoidable in many industrial applications. These harsh environments may involve extreme physical conditions, such as high-temperature, high-pressure, corrosion, toxicity, strong electromagnetic interference, and high-energy radiation exposure. Due to these severe environmental conditions, conventional temperature sensors are often difficult to apply. This situation has opened a new but challenging opportunity for the sensor society to provide robust, high-performance, and cost-effective temperature sensors capable of operating in those harsh environments.

One example representing such harsh environments is an entrained flow slagging gasifier, which is one process among the coal gasification community that has received strong attention in recent years to help meet the growing demand for energy in a cost effective and environmentally friendly manner. Coal gasification is used today not only in refineries and chemical plants, to produce fuels, chemicals and fertilizers, but also for electric power generation, which is a way to generate extremely clean electricity and other high-value energy products. In the entrained flow slagging gasifier, rather than burning coal directly, coal gasification reacts coal with steam and carefully

controlled amounts of air or oxygen under high temperatures and pressures. This releases large amounts of alkali, sulfur, silica, steam, transition metals, and a host of other corrosive agents that are present to a greater or lesser extent depending upon the source of the coal and the operation condition of the gasifier unit. For temperature sensors, which must operate in the high temperature sections of the gasifier unit, the corrosion can be extremely severe.

Long term stability of the temperature measurement system relies on providing suitable protection of the sensor element from the corrosive environment of the gasifier. Long life and stability of the temperature sensor is highly desired to ensure the continuous operation of the coal gasification system. In this high temperature and chemically corrosive environment, rather limited high temperature measurement techniques, such as high temperature thermocouples and optical /acoustic pyrometers, are available. Current high temperature thermocouples that utilize precious metals drift significantly and have a limited life of only a few days because of its susceptibility to attack from alkali vapors and transition metals in the gaseous or solid byproducts of the coal reaction.Slag buildup around the thermocouple is also a problem, forming an insulating layer on the thermocouple increasing the corrosion and changing the temperature measurements. In non-contact optical pyrometers, an infrared-transparent high temperature window on the gasifier wall is necessary to maintain the large pressure differential, while allowing transmission of the infrared radiation emitted by the product gases to the detector placed outside the gasifier. Obstruction of the sight-path opening for the pyrometers in the

refractory wall by molten slag is a major problem. Shifting of the refractory lining, which could have a thickness of 2 feet or more, during heat-up and operation could also cause blockage of the sight path.

In addition, the measurement is also subject to interference from the radiation emitted by entrained particles or the relatively cold refractory walls. Acoustic pyrometers, which deduce gas temperature along a line of sight by measuring the speed of sound along that line, have also been evaluated for use in gasifiers. Noise in the plant or gasifier, such as from the high velocity burners, soot-blowers, etc., also interferes with acoustic temperature measurements. This situation suggests that innovative techniques that operate in the gasifier harsh environment for real-time, reliable monitoring of temperature be developed.

In this research program, several optical high temperature measurement instruments based on single crystal sapphire material have been designed and tested for on-line, real-time, reliable, long-term monitoring of temperatures inside the coal gasification environment, which includes sapphire fiber extrinsic Fabry-Pérot interferometric (EFPI) sensor; intensity-measurement based polarimetric sapphire sensor and broadband polarimetric differential interferometric (BPDI) sapphire sensor.

By employing the high melting point and chemically inert single-crystal sapphire material, combined with the enormous advantages of optical sensors, such as immunity to

electromagnetic interference (EMI), non-polluting to the environment, resistance to chemical corrosion, avoidance of ground loops, high sensitivity, huge bandwidth, capability of remote operation and etc. The designed optical sensor can be potentially applied in those harsh environments, where high temperature, high radiation exposure and chemically corrosive conditions exist, such as in coal gasifiers, nuclear power plants, etc.

More detailed treatment of the related research will be presented in Chapter 2. Chapter 3 provides information on the employed major optical materials for the sensing system design, namelye single-crystal sapphire and fully stabilized single crystal zirconia. Those materials are not only capable of surviving the high temperature and extremely chemically corrosive environments, but also their optical properties offer a good solution for the designed optical sensor. The principles of those designed optical sensors are presented in chapter 4, including optical sensing heads design, i.e. sapphire fiber EFPI (extrinsic Fabry_Parrot interferometric) sensor head and polarimetric sensor head, and the potential optoelectronic signal processing units, which are SCIIB (self-calibrated interferometric/intensity based) processing unit, intensity measurement based polarimetric detecting unit and white-light spectral signal processing unit. Chapter 5 provides the experimental results that have been performed to date based on different optical sensing schemes. Chapter 6 describes the future work on the optical temperature sensing instruments.

Chapter 2. Background of the proposed research

Coal is the most abundant natural resource for industrial heating power production applications. Coal gasification represents the next generation of coal-based energy production, and is a way to generate extremely clean electricity and other high-value energy products. Direct measurement of temperature in coal gasifiers requires a sensor technology that can withstand the extremely harsh environment posed by the high temperatures and corrosive agents present in these systems. This proposed research is to address this critical need, and supported by NETL (National Energy Technology Laboratory), U.S. Department. of Energy. This work is performed in collaboration with Global Energy Technology, Inc, a partner in the Wabash River Coal Gasification Repowering Project Joint Venture.

2.1 Industry needs for this research

In order to meet the requirements of the Clean Air Act while promoting the efficient use of reserved coal resources, industry and government in the United States has responded by the development of new technologies for the utilization of coal under the Clean Coal Technology program. One such initiative has been the adoption of the use of coal gasification techniques to generate extremely clean electricity and other high-value energy products. This technique historically was used in refineries and chemical plants to produce fuels, chemicals and fertilizers [1-2]. Coal gasification offers a much more efficient way to generate electricity than conventional coal-burning power plants. In a conventional plant

heat from the coal furnace is used to boil water, creating steam to drive a steam-turbine generator which in turn produces the electric power. By contrast, rather than burning coal directly, coal gasification reacts coal with steam and carefully controlled amounts of air or oxygen under high temperatures and pressures. A gasification-based power plant uses the hot, high-pressure coal gases exiting a gasifier to power a gas turbine. Hot exhaust from the gas turbine is then fed into a conventional steam turbine, producing a second source of power. This unique integrated gasification combined cycle (IGCC) configuration of turbines offers major improvements in power plant efficiencies compared with conventional coal combustion. Today's conventional combustion plants are typically 33-35% efficient (fuel-to-electricity). Coal gasification offers the prospects of boosting efficiencies to 45-50% in the short-term and potentially to nearly 60% with technological advancements.Besides high thermal efficiency, this process has also been demonstrated to be capable of significant reduction in CO_2, NO_X, and sulfur emission when compared to conventional coal burning power plants. Another advantage of the IGCC plant is the ability to utilize a wide range of feedstocks, including coal, biomass, and wood wastes.

As new emerging coal-fired power plants for advanced power generation, these integrated gasification combined cycle (IGCC) plants offer the potential to be competitive with all other power systems from a cost and performance standpoint. But for electric power generation, the technology is still in the demonstration phase, they must first undergo replication to reduce cost and optimize performance, even coal gasification has been successfully demonstrated to produce fuels, chemicals and fertilizers in refineries and chemical plants. To optimize performance for these IGCC plants, certain

important physical parameters should be monitored and controlled precisely for coal gasification processes, such as real-time accurate and reliable monitoring of temperatures at various locations in a coal gasifier [3], pressure distribution monitoring in a gasifier, burning material flow patterns inside the gasifier control and monitoring, air or oxygen monitoring, and etc.

One of these challenges to optimize performance for the coal gasification process is to perform real-time measurement of the gasifier temperatures, which is an important control parameter in the operation of an entrained flow slagging gasifier. The gasifier must be operated at a temperature high enough for the ash in the fuel, such as coal, to melt and to be fluid enough to flow out of the gasifier through the bottom tap-hole. Load changes will also affect the temperature in the gasifier and downstream, and would require adjusting the operating conditions. Operating at too low a temperature would cause the molten slag to become viscous or freeze, plugging up the tap-hole and preventing additional slag from draining out of the gasifier. Eventually the gasifier has to be shut down, cooled off, and the slag, now in the form of a hard vitreous rock, has to be manually chipped out to be removed from inside the gasifier. The shut down to clean up the slag may take weeks, resulting in a lengthy loss of production. On the other hand, operating at too high a temperature would significantly shorten the life of the refractory lining. In addition, more of the alkali species in the ash would be volatilized, reacting with the ash particles entrained in the gas to form low temperature eutectics which deposit in the cooler sections of the gasifier or on downstream equipment, such as the boiler, causing plugging problems. Operating the

gasifier at too high a temperature will also reduce the conversion efficiency of the gasification process in the production of the synthesis gas.

Most entrained flow gasifiers use oxygen as the oxidant. Coal is ground into slurry or pulverized, and injected into the gasifier with oxygen and steam at high velocity. The flow condition inside the gasifier is highly turbulent, with many pockets of gas recirculation zones. Temperature in various regions of the gasifier could be widely different. The temperature at the exit of the burners could be above $1927^\circ C$ (3500F), whereas close to the wall temperature could drop to less than $1316^\circ C$ (2400F).

In order to realize the full economic potential of gasification systems there is an increasing need to utilize a wide variety of feedstock in addition to coals, such as biomass, refuse, wood wastes, etc., in the gasification plants. The ash properties of these various feedstocks vary significantly, and would require operating the gasifier at different temperatures to facilitate slag tapping. Real-time accurate and reliable monitoring of temperatures at various locations in a gasifier is thus highly desirable. However, due to the harsh environment involving entrained molten slag, high temperatures and pressures, and corrosive gases, conventional sensors and measurement devices are very difficult to apply [4-8].

Various methods have been investigated in the past [9-13]. Among these are optical and acoustical pyrometers, and high temperature thermocouples. In the non-contact optical pyrometers, an infrared transparent high temperature window on the gasifier wall is necessary to maintain the large pressure differential, while allowing transmission of the infrared radiation emitted by the product gases to the detector placed outside the gasifier.

Obstruction of the sight-path opening for the pyrometers in the refractory wall by molten slag is a major problem. Shifting of the refractory lining, which could have a thickness of 2 feet or more, during heat-up and operation processes could also cause blockage of the sight path. In addition, the measurement is also subject to interference from the radiation emitted by entrained particles or the relatively cold refractory walls. Acoustic pyrometers, which deduce gas temperature along a line of sight by measuring the speed of sound along that line, have also been evaluated for use in gasifiers. Noise in the plant or gasifier, such as from the high velocity burners, soot-blowers, etc., also interferes with acoustic temperature measurements.

Direct contact temperature measurement is preferred since it will give the measurement for a specific location. Several of these devices installed at critical locations inside the gasifier could provide a temperature profile of the gasifier. Flow patterns inside the gasifier could be deduced from the temperature profile, and performance of the gasifier could be monitored and improved by making operating adjustments. However, no direct contact measuring device is available to date due to material issues. The highly corrosive molten slag attacks both metals and ceramics. Ceramic materials are also susceptible to attack from alkali vapors in the gas [14-18]. Current high temperature thermocouples that utilize precious metals drift significantly and have a limited life of only a few days. Slag buildup around the thermocouple is also a problem, forming an insulating layer on the thermocouple. This situation suggests that innovative techniques for real-time, reliable monitoring of temperature be developed that can operate for long periods in the harsh environment of the gasifier.

2.2 Non-optical temperature measurement techniques review

In science, temperature can be defined in terms of the heat transferred in a Carnot cycle. This is generally not the most practical way to measure temperature and in practice many different techniques are used depending on the temperature measurement requirements. Theoretically speaking, all temperature measurements are indirect. That is to say, that every temperature measurement involves the use of some type of calibrated transducer to convert a measurable quantity into a temperature value. Those transducers are the parts of the temperature sensors that convert changes in temperature into other measurable physical quantities, such as volumetric expansion (liquid-filled thermometer), dimensional change (bimetallic thermometer), EMF-electromotive force (thermocouple), resistance (resistance temperature detector, or RTD), radiated energy (radiation thermometer), or some other characteristic of a material that varies predictably and reproducibly with temperature [19-20]. However, in industrial process measurement and control, the concept of direct and indirect temperature measurement has a different meaning. A direct measurement is a measurement of the temperature of the product itself. An indirect measurement is a measurement of some other parameter from which one can infer the product temperature.

Temperature may be measured using any physical system with an extrinsic property related to its temperature. The overwhelming majority of temperature measurements are made using only a few basic types of instrument: liquid-in-glass thermometers, thermocouples, resistance thermometers and radiation thermometers. These conventional

and traditional measurement instruments have been in use for several decades, and the major sources of instability or drift, as well as possible systematic errors, are well understood. Further, there is extensive industrial experience with these techniques, which allows the user to design a reliable system with a high chance of success. These traditional techniques also offer the advantage of having a large range of suppliers offering equivalent plug compatible equipment in product ranges, product support and replacements are unlikely to be a problem. As mature technologies, they are also generally much cheaper.

There is a continuing stream of new instrumentation techniques entering the market due to the increased availability of technologies as a spin-off from the electronics and computer industries. Advances in communications technologies have made laser sources and optical fibers cheap, reliable and readily available. Many of the unconventional thermometry techniques require complex processing of the signals received from the sensor. The availability of cheap computers integrated into the measurement equipment enables the often complex processing associated with the more unusual sensors to be made available to the user.

These newer techniques may offer the promise of doing a much better job than traditional techniques. Also, generally speaking, these "unconventional" techniques in thermometry have been developed in response to a specific measurement problem for which the commonly used traditional techniques are not suitable. Those specific measurement requirements become quite popular in today's modern industry environments, such as

low thermal mass sensors for fast time response, gas temperature measurement, measurement of internal temperature profiles, measurements in hostile environments, e.g., EMI (Electro-magnetic interference), radiation, corrosion and intrinsic safety, where the measurement environment should not be affected by measurement units, optical sensors are easily able to satisfy these requirements.

As discussed in last section, those conventional and traditional measurement instruments cannot be easily applied because of the high temperature and chemically corrosive environment in coal gasifier. Limited high temperature measurement techniques such as pyrometry and optical /acoustic measurement techniques are available each with their own limitations. The potential thermometry technique candidates for this harsh environment will be reviewed in the following sections.

Table 2.1. The common sensor used in temperature measurement, each one utilizing physical properties that change with temperature[20]:

Sensor	Transducer property	Measured quantity
Mercury in glass thermometer	Thermal expension	Length
Constant volume gas thermometer	Thermal expension	Pressure
Platinum resistance thermometer	Electrical resistance	Resistance
Thermocouple	Seeback coefficient	Voltage
Optical pyrometer	Thermal radiation	Radiant flux
Acoustic thermometer	Sound velocity	Time

| Noise thermaometer | Johnson noise | Power |
| Thermo-luminescent thermometer | Luminescence decay | time |

2.2.1 High temperature thermocouple

A thermocouple is an assembly of two wires of unlike metals joined at one end, the hot end, and at the other end, the cold junction, the open circuit voltage is measured. This voltage (electromotive force, or EMF), also called Seebeck voltage, depends on the difference in temperature between the hot and the cold junction and the Seebeck coefficient of the two metals. The Seebeck EMF develops when there are differences in temperature between junctions of dissimilar metals in the same circuit. Also known as the thermoelectric effect, German physicist J.T. Seebeck discovered the phenomenon in 1821. The Seebeck EMF depends on the characteristic of the thermocouple metals and the temperature difference between the measuring and cold junctions. A measurement indicates the temperature of the hot junction when one knows the cold junction temperature or when measurement circuitry compensates for cold junction temperature.

The highly corrosive molten slag attacks both metals and ceramics in the coal gasifier. Current high temperature thermocouples that utilize precious metals drift significantly and sensor probe have a limited life of only a few days. Slag buildup around the thermocouple is also a problem, forming an insulating layer on the thermocouple.

2.2.2 Acoustic methods

A wide range of thermometers have been based on the temperature dependence of the speed of sound in a material [21, 22]. Solids, liquids and gases have been used as the temperature sensor. For certain cases, it is difficult to measure the temperature of a gas using inserted probes, due to the low thermal mass and low conductivity of gases and, at high temperatures, the strong radiation coupling of the sensor to the walls of the enclosure. Using the gas itself as the temperature sensor overcomes these problems. The uncertainty claimed for the method is typically 30^0C at $1000\ ^0C$.

The main difficulty with the technique is that the speed of sound is also strongly dependent on the composition of the gas along the path, which is generally not constant in a combustion chamber. Further, soot particles slow the wave significantly, and will result in a large error. Another problem arises from refraction of the sound wave front by density and temperature gradients in the chamber. These are often turbulent and mix the wave front, making accurate time of flight determinations difficult. Since the sound travels with the gas, the apparent sound speed will also be strongly affected by the flow velocity. Practical systems usually compensate for this by performing measurements in both directions.

The technique has been used to measure temperatures over 5000^0C. However, the gas density is then very low, and thus the sound speed becomes high. The time delay is then dominated by propagation through the cooler regions of gas around the measurement

region and the contribution from the 'hot' region becomes increasingly difficult to disentangle.

2.2.3 Gas-viscosity thermometry

An interesting class of thermometric devices was developed in the late 1970's, relying on the temperature dependence of the viscosity of a gas. In this kind of sensor, a constant flow of neutral gas down a relatively wide tube is throttled at the sensor tip by a narrow constriction, before returning to the gas handling system. The system is designed to maintain a laminar-flow regime in the capillary, so that for a given flow rate, the pressure drop across the probe is roughly proportional to the gas viscosity. The flow resistance of the gas feed lines to and from the capillary sensor is small compared to that of the capillary. Over a wide range, the gas viscosity is a fairly linear function of temperature. So, for example, a typical gas-viscosity probe exhibits a pressure drop of 10 kPa at 1000^0C increasing to 15 kPa at 2000^0C. Argon is used as a working gas for metal capillaries, such as tungsten, molybdenum or tantalum, whereas air is used for ceramics, such as zirconia or alumina.

The chief advantage of the system is that only the mechanical integrity of the capillary need be ensured, which allows a much wider choice of materials, suited for long use at high temperatures, than for electrical sensors. Gas-viscosity sensors have been used for extended periods up to 2300^0C. The main disadvantages are the need for a relatively complex gas-handling system and the relatively large uncertainty of about 1%.

2.3 Optical temperature measurement technique review

Optical sensors are devices in which an optical signal is changed in some reproducible way by an external physical stimulus such as temperature, pressure or strain. An optical beam is characterized by several variables such as intensity, wavelength spectrum, phase and state of polarization, many different physical phenomena related to these characterizations are used to perform the sensing. Temperature sensors probably constitute the largest class of commercially available optical sensors.

Advances in communications technologies have made laser sources and optical fibers cheap, reliable and readily available. Besides bulk optics based sensors, a wide variety of temperature sensors using optical fibers have been developed [23]. They offer several significant advantages over electrically based sensors, such as small sensor size, lightweight, electro-magnetic immunity, and etc.

The main physical techniques in use in optical thermometry are remote pyrometry (or radiation thermometer), Fabry-Pérot interferometers to measure optical path-length changes in a material, Raman scattering, and rare-earth fluorescence and fluorescence decay time monitoring.

Remote pyrometry.

All materials emit thermal radiation (radiant heat) and the amount of thermal radiation

emitted increases with temperature. The measurement of the amount of thermal radiation emitted by a material can therefore be used as an indicator of its temperature. Instruments designed to measure temperature in this way are called radiation thermometers. The basic operating principle of radiation thermometers [24] is to measure some part of the thermal radiation emitted by an object and relate it to the temperature of the object using a calibration curve that has been determined either experimentally or theoretically (from Planck's law). Typically this is used in high-temperature applications because the intensity of the spectral radiation emitted decreases by the fourth power as the tmerpature is lowered.

By using fiber optics, radiation thermometry optical-fiber sensors convert the end of the fiber into a small black-body cavity, by shearing it at an angle and coating it with metal, such as platinum, for use as a radiation thermometer. Since the fiber can be very small (<100 μm) and the sensor diameter is the same as that of the fiber itself, such probes can have response times less than 0.1 s.

Thermal expansion thermometers.

There are temperature sensors that use the temperature dependence of the optical path length in a small optical resonator cavity, i.e a Fabry-Pérot (FP) interferometers at the end of an optical fiber [25]. These temperature sensors measure the change in optical path length of a short piece of material whose thermal expansion coefficient and refractive index as a function of temperature are known. Several approaches have been tried for the

sensor resonator itself. A short length of sapphire fiber or silicon fiber may be used, allowing many hundreds of wavelengths to be present, and giving extremely high sensitivity to temperature. In this case, many maxima and minima will occur over the usable range of the sensor and fringe-counting techniques must be used to keep track as the temperature is changed.

Thermoluminescence thermometers.

They use the temperature dependent decay time or intensity of a UV stimulated visible fluorescence pulse. In sensors based on thermoluminescence, a UV light source in the processing "head" of the system is focused into an optical fiber, thus illuminating a small sample of thermoluminescent phosphor at the end of the fiber. Some of the most commonly used phosphors are made using a rare-earth, such as gadolinium or europium, doped into a ceramic crystal, such as yttria[26-28]. The strong temperature dependence of luminescence allows good resolution, some claiming less than 0.1 ^{0}C, although the wide range of time constants (or intensity) over the usable temperature range for the phosphors leaves these instruments with much poorer linearity than this. Such sensors have found application in the measurement of temperatures within microwave ovens, or in very high-magnetic fields.

Rayleigh scattering thermometers.

Another class of fiber-optic temperature measurement devices exploits the temperature

dependence of scattered light within a fiber [29]. Rayleigh scattering, resulting from scattering from impurities in the fiber has a similar spectrum to the incident laser beam and is not relevant here. Raman scattering, however, results from the scattering of light off phonons, or vibrational modes of the crystal, and results in two wavelength-shifted scattered-light signals. One, at a longer wavelength than the incident light, resulting from phonon emission, is called "Stokes scattering", and the other, at a shorter wavelength, resulting from phonon absorption, is called "anti-Stokes scattering". The intensity of the anti-Stokes scattering depends strongly on the number of sufficiently energetic optical phonons in the crystal, which is a strong function of temperature. The ratio of the anti-Stokes to Stokes scattering is thus a sensitive indicator of temperature.

2.4 Temperature sensors developed in this research

CPT proposed and developed three different temperature-sensing schemes for single crystal sapphire based sensors, because of the inherent advantages of single crystal sapphire's chemical inertness and high melting temperature (over 2000°C). These are sapphire fiber extrinsic Fabry-Pérot interferometric (EFPI) sensor [30], intensity-measurement based polarimetric sapphire sensor and broadband polarimetric differential interferometry (BPDI) sapphire sensor [31].

Those sensors will be described in detail in the following chapters, based on comparative evaluation and analysis of the experimental results, the broadband polarimetric differential interferometry (BPDI) sapphire sensor was chosen for further prototype

instrumentation development. This approach is based on the self-calibrating measurement of the differential optical path length in a single-crystal sapphire sensing element, which is a function of temperature. A complete prototype sensor system was designed, fabricated and tested.

Chapter 3. Properties of single crystal sapphire

In a coal gasifier as well as other industrially harsh environments, temperature-related degradation mechanisms include thermal shock due to rapid thermal cycling, and corrosion resulting in lower melting point or high thermal expansion coeeficeint phases . All these factors must be considered in elevated temperature design. Single crystal sapphire and fully stabilized zirconia were chosen due to their optical properties, high mechanical strength, temperature stability, wear resistance and chemical inertness.

Possessing a high melting temperature (over 2000 $^{\circ}$C) and good mechanical properties, chemically inert single-crystal sapphire and fully stabilized zirconia are attractive candidates to be employed under adverse conditions, such as organic solvents and acids, at elevated temperatures and chemically corrosive environments. In the designed sensors, a single crystal sapphire tube is employed to protect sensing element from corrosive environment, the sensing element itself is also made of single crystal sapphire.

3.1 Single-crystal sapphire growth methods

Single-crystal aluminum oxide (α-Al$_2$O$_3$), better known as sapphire, is currently the material of choice for infrared windows and domes that must survive in the most demanding environments. The heat exchanger method (HEM)[32-36] is one way in which sapphire is grown. In this technique, aluminum oxide is heated above its melting

point of 2040^0C in a molybdenum crucible containing a single-crystal sapphire seed at the bottom. The seed is mounted on a cold finger that is cooled by helium gas. Evacuation of the furnace permits volatile impurities to escape prior to crystallization, which is begun at the seed by lowering the furnace temperature and increasing the coolant supply to the cold finger. The entire charge solidifies over several days, after which it is annealed just below the melting point to remove residual stress. A very slow cooldown results in a huge, stress-free single crystal.

Since it is a very hard material, sapphire is difficult and expensive to cut and polish. It was estimated that polishing a sapphire dome costs as much as growing the single-crystal material. It is therefore desirable to grow sapphire in the shape of a hemisphere to minimize the amount of grinding required to attain the final dimensions.

An important near-net-shape process for sapphire is edge-defined, film-fed growth, called the EFG method [37-41]. In this technique, a seed crystal is dipped into the top of a capillary tube containing molten aluminum oxide. The shape of the capillary determines the shape of the resulting crystal. A round capillary gives a continuous sapphire filament. A thin rectangular capillary gives a flat sapphire ribbon or sheet, while a tubular capillary gives a tube-shaped rod.

Although the crystal quality of EFG sapphire is good, it is not as good as that of HEM sapphire, which is grown much more slowly and annealed in situ prior to removing the

boule from the furnace.

3.2 Optical properties

Many optical sensing applications require IR transmission, especially for thermal optical sensing. Most broadband IR window materials don't tolerate even moderate temperatures and are hygroscopic at high temperatures. As they absorb water, they become less efficient at transmitting IR light. The use of sapphire avoids these problems. Sapphire's lower surface scattering losses at IR wavelengths also translate into less rigorous surface finish requirements.

Single crystal sapphire increases transmission capability over that of glass and quartz. The transmission is equal to or greater than 80% from a wavelength of 30 microns in the UV, through the visible range of 0.4-0.7microns to 5.5microns in the IR. The perfection and purity of the UV grade sapphire crystals offer a transmission capability superior to that of standard- grade sapphire. Figure 3.1 shows the transmission band for a window thickness of 1mm(.039 in) thick provides a nearly uniform transmission of 85%[42].
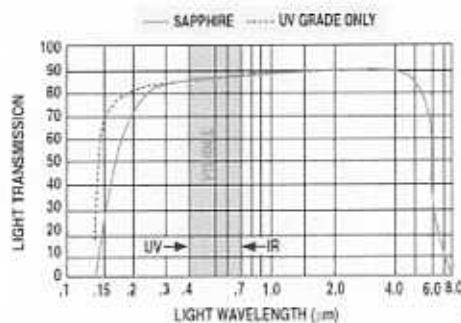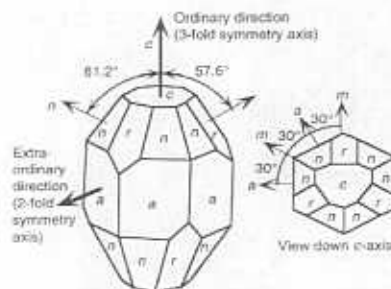
Fig 3.1.　　　　　Fig 3.2.

Figure 3.1. The approximate transmission bands of standard- and UV-grade sapphire are plotted for a window thickness of 0.039 in.

Figure. 3.2. Sapphire crystal showing 3-fold-symmetric *optical axis* (ordinary direction) and 2-fold-symmetric extraordinary direction. Sapphire crystal cleavage faces are customarily designated c, n, rand a, as indicated. When viewed down the 3-fold c-axis, directions designated a and m alternate every 30^0.

Single crystal sapphire, witht its hexagonal inner structure, has two principal dielectric constants, hence two refractive indices. Such materials are called uniaxial, the unique crystallographic axis is the C-axis, also called optical axis. One method to denoting the two unique principal axes is to state the orientation of the electric field (E) relative to the optical axis. The dielectric constant for E normal to C-axis, this circumstance is called ordinary ray, refractive index is no, the other dielectric constant E parallel to C-axis, called extraodinary ray, ne. For sapphire, since ne-no<0, it is called negative unaxial crystal. The 3-fold symmetry axis in Fig. 3.2 [42] is designated as the c-axis in the sapphire crystal. It is also called the optical axis or the ordinary direction. The 2-fold symmetry axis perpendicular to the 3-fold axis is called the a-axis or the extraordinary direction.

Room-temperature dispersion formula[43]:

$$n_o^2 - 1 = \frac{1.4313493\lambda^2}{\lambda^2 - 0.0726631^2} + \frac{0.65054713\lambda^2}{\lambda^2 - 0.1193242^2} + \frac{5.3414021\lambda^2}{\lambda^2 - 18.028251^2}$$

$$n_e^2 - 1 = \frac{1.5039759\lambda^2}{\lambda^2 - 0.0740288^2} + \frac{0.55069141\lambda^2}{\lambda^2 - 0.1216529^2} + \frac{6.5927379\lambda^2}{\lambda^2 - 20.072248^2}$$

(3.1)

Table 3.1 Parameters for room temperature infrared absorption edge[43]

	A(cm^-1)	γ	v_0(cm^-1)
o-ray	55,222	5.03	900

	94,778	5.28	914
e-ray	33,523	4.73	871

3.3 Thermo-optic effects

Temperature is one of the main factors affecting the refractive index of solids, the thermal-optical coefficients dn/dt can be estimated from a devation of the Clausius-Mossotti relations [43]:

$$\frac{1}{(\varepsilon-1)(\varepsilon+2)}(\frac{\partial\varepsilon}{\partial T}) = -\alpha\left[1 - \frac{V}{\alpha_m}(\frac{\partial\alpha_m}{\partial V})_T\right] + \frac{1}{3\alpha_m}(\frac{\partial\alpha_m}{\partial T})_v, \qquad (3.2)$$

Where α_m is the macroscopic polarizability, where α_m is the macroscopic polarizability, α is thermal expansion coefficient, ϵ is the dielectric constant, and V is the geometrical volume of the material,. The first two terms are the principal contributors in ionic materials: a positive thermal expansion coefficient α results in a negative thermo-optic coefficient and a positive change in polarizability with volume results in a positive thermo-optic coefficient. In ionic materials with a low melting point, thermal expansion is high and the thermo-optic coefficient is negative (typical of alkali halides); when thermal expansion is small (indicated by high melting point, hardness, and high elastic moduli), the thermo-optic coefficient is positive, dominated by the volume change in polarizability (typical of the high temperature oxides). Thermal expansion has no frequency dependent but polarizability does. At frequency(wavelengths) near the edge of

transparency, the polarizability(and $d\alpha_m/dV$) rises and dn/dT becomes more positive(or less negative).

Because of the symmetry of the atomic arrangements in the structural units for the single crystal sapphire, it exhibits differences in the speed of propagation of light along different crystallographic axis. This difference in the speed of propagation of light with respect to the different crystallographic axis is termed birefringence. Since the electron probability density distribution is related to the spacing between adjacently bonded atoms, and since the propagation speed of light in a particular direction in a crystal is a function of the electron density distribution, as the spacing between atoms changes the speed of light propagation changes. Since the thermal expansion coefficients of sapphire are different along the a and c crystallographic directions, the change in spacing between adjacent atoms in each of these directions will be different for a given temperature change. This suggests that the magnitude of the birefringence of the single crystal sapphire fiber will change with temperature.

3.4 Mechanical properties

Sapphire provides superior electromechanical, thermal, and chemical properties compared with glass or quartz. Sapphire's properties include extreme hardness, high strength, good thermal characteristics, and chemical inertness. On the Mohs scale of hardness, which assigns a unit of 10 to diamond, sapphire is rated at 9, quartz at 7, and glass at 4.5–6.5[42]. In contrast to other available light-transmitting materials, sapphire

offers maximum resistance to abrasion and scoring. It also provides a durable surface with a low coefficient of friction that minimizes the accumulation of undesirable bubbles and process scum.

The compressive strength of sapphire is 300,000 psi, nearly double that of quartz. Its modulus of elasticity (Young's modulus) is 50–56 at 106 psi—five times that of quartz. Sapphire is an ideal material for windows that must withstand great pressure or vacuum. Empirical hydrostatic burst data for sapphire (which includes a safety factor of 3) has been calculated for circular window diameters from 0.125 to 2.000 in. and over a range from 0.020 to 0.200 in. thick (see Figure 3.3 [42]).
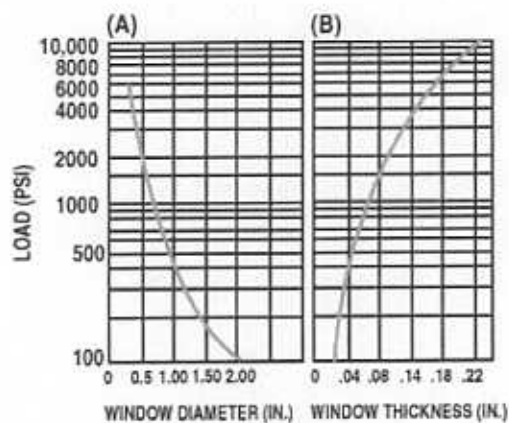
Figure 3.3. Sapphire windows that are 0.080 in. thick permit safe operation at pressure loads from 100 to 6000 psi over diameters ranging from 2 to 0.25 in. (A). Sapphire windows of 0.0500 in. dia. resist pressures from ~100 psi at 0.020 in. thickness to ~7500 psi at 0.200 in. thickness (B).

It has excellent resistance to erosion by liquid and solid particles, can operate at high temperature, and can survive high stress induced by rapid heating. However, the resistance to thermal stress is limited by a loss of mechanical strength at elevated temperature [44-48]. At temperature above 400 °C a dramatic decrease in sapphire's compressive strength along the c-axis occurs due to the activation of deformation twinning on rhombohedral planes. Efforts in recently year focused on characterizing the

strength of sapphire for engineering design and improve the high temperature strength.

Various ways to increase the strength of sapphire were explored, including heat treatments, doping and improvement of fabrication techniques [49-50].

The variable effect of different polishing procedures on mechanical strength is one of the most vexing problems in engineering with optical materials. The most variable factor governing the mechanical strength of an optical ceramic is the surface finish. Both grinding and polishing procedures have a significant effect on biaxial strength of sapphire windows. Using more aggressive grinding procedures can introduce deep subsurface damage that will be hard to remove during subsequent polishing. Usually, the finer the grit used to grind a surface, the stronger is the resulting ceramic [51].

Table 3.2 Thermal properties of single crystal sapphire[42]

Temperature(K)		Heat capacity(J/g.k)	Thermal Expansion(10^{-6}/K)	Thermal conductivity(W/m.k)		
Debye	Melt			@250K	@300K	@500K
1030	2319	0.777	6.65//a 7.15//c	58	46	24.2

3.5 Chemical inertness

Sapphire is more chemically inert than glass and is unaffected by acids, strong alkalis, or organic solvents. These characteristics - combined with high temperature stability - make the sapphire windows ideal for use in applications where long, useful life is critical.

Sapphire's chemical inertness in the presence of a wide variety of reagents at temperatures greater than 1000°C make it ideal for chemical industrial applications. For example, silica becomes soluble in hydrofluoric acid at room temperature, but sapphire exhibits no solubility in alkalies or acids, including hydrofluoric acid. At elevated temperatures, other acids (e.g., hydrochloric acid and nitric acid) attack silica, but not sapphire [42].

3.6 Zirconia

Pure Zirconia (Zirconium dioxide) has a high melting point (2700°C) and a low thermal conductivity. Its polymorphism, however, restricts its widespread use in ceramic industry. During a heating process, zirconia will undergo a phase transformation from the monoclinic to the tetragonal phase. The change in volume associated with this transformation makes the usage of pure zirconia in many applications impossible. Addition of some oxides, such as CaO, MgO, and Y_2O_3, into the zirconia structure in a certain degree results in a solid solution, which is a cubic form and has no phase transformation during heating and cooling. This solid solution material is termed as stabilized zirconia, a valuable refractory [42].

Stabilized zirconia is used as a grinding media and engineering ceramics due to its increased hardness and high thermal shock resistance. Stabilized zirconia is also used in

applications such as oxygen sensors and solid oxide fuel cells due to its high oxygen ion conductivity.

Single-crystal windows with a cubic crystal structure, such as zirconia, are preferred over noncubic crystals to reduce optical scatter. As light passes from one randomly oriented grain to another inside a polycrystalline window containing noncubic crystals, the light is refracted and reflected at each grain boundary. In cubic materials, the refractive index is constant, regardless of crystal orientation. As light passes from grain to grain of a polycrystalline cubic material, no refraction or reflection (i.e., no scatter) occurs.

Chapter 4. Working principles of the designed optical sensors

A sensor measurement system is typically composed of some basic elements: a sensing element, i.e transducer, a unit to convert measurand into measurable physical signals; signal conditioning and processing elements and software, such as detection units, signal amplifiers, supporting electronics such as current transmitters, oscillators, signal A/D converter, computer systems, computer software for signal processing calculations and control, and data presentation elements. This chapter is devoted to those separate elements designs, which will be categorized as sensing elements, i.e optical transducer design in section 1, the detecting units in section 2, and section 3 for supporting subsystems design, including blackbody radiation elimination subsystem and a temperature acquisition subsystem for referencing.

4.1 Optical sensing elements design

Optical sensors are devices in which an optical signal is changed in some reproducible way by an external physical stimulus such as temperature, pressure or strain and etc. An optical beam is characterized by several variables such as intensity, wavelength spectrum, phase and state of polarization, many different physical phenomena related to these characterizations are used to perform the sensing. For temperature measurements, the interferencing phenomena is widely employed to design high sensitivity optical sensors, other techniques related to optical methods such as thermal imaging and light scattering methods and etc, are also viable

There are several different types of interferometric techniques which have been used to measure temperatures and other physical parameters. These are the Mach-Zehnder[52], Michelson, Fabry-Perot, and Sagnac interferometers. Optical fiber Fabry-Perot sensors are highly sensitive to temperature, mechanical vibration, magnetic fields, and acoustic waves [53-54]. Many techniques have been used to create intrinsic or extrinsic Fabry-Perot cavities, such as Bragg gratings in or on the fiber, metal coatings on the end faces of the fiber, and the use of air-glass interfaces at the fiber ends as the reflectors.

Although intrinsic Fabry-Perot sensors have been used in the past to measure several physical parameters including temperature, extrinsic Fabry-Perot interferometers (EFPI) have shown their ability to be immune to fiber optic polarization and only sensitive to axial strain components, which gives them an advantage over other electro-mechanical and intrinsic Fabry-Perot sensors.

In this research work, sapphire fiber based EFPI (extrinsic Fabry-Perot interferometric) sensor is designed and tested first. Another sensing element design is to use the intrinsic "cavity" in a bulk sapphire disk, the so called cavity is actually generated by birefringence and dimensional thickness of the sapphire disk, which is really the difference of optical paths between two orthogonal linearly polarized lights in the sapphire disk. The optical path difference corresponds to the differential phase delay between two orthogonal polarized lights.

4.1.1 EFPI sapphire fiber sensor

Thermally bonded silicon fiber EFPI sensors have shown great promise for measuring temperatures (and other physical parameters) below 800°C and have been designed and tested extensively in CPT. While at higher temperatures the devices degrade rapidly, the degradation mechanisms fall into two general categories, either crystallization of the silica cladding region occurs or diffusion of the germanium dopant (used to establish the refractive index gradient between the core and the cladding) from the core region into the cladding changes the waveguiding properties of the fiber. By replacing silicon fiber with sapphire optical fibers, the sensors can potentially operate at high temperature (up to 1500°C) environment[30]. The first attempt in this program is focused on investigating single crystal sapphire based Fabry-Perot temperature sensors for ultrahigh temperature measurement in coal gasification systems.

As shown in Figure 4.1, a sapphire air gapped EFPI sensor head is formed by inserting the lead-in single crystal sapphire fiber into the one end of the sapphire tube and inserting another short piece of sapphire fiber into the other end of the tube to act as the reflecting surface (target fiber). Both the lead-in and the target sapphire fiber ends are polished to optical quality. While one end of the target sapphire fiber is highly polished, the other end is shattered to prevent any significant reflection that would interfere with the measurements. The light propagating in the lead-in sapphire fiber is partly reflected (7%) at the first sapphire-air boundary. The transmitted light travels through the air gap and is also partially reflected (7%) at the end face of the target sapphire fiber. Reflectance R is determined by the following equation:

$$R = [\frac{(n - n')}{(n + n')}]^2, \qquad\qquad (4.1)$$

where n is the refractive index of the sapphire fiber, and n' is the refractive of the medium forming the cavity between two fibers, which is 1 for the air.

An interference signal is generated by these two reflected waves and the phase difference depends on the length of the air gap. The interference signal is detected by a spectrometer and processed in a computer, in this way the absolute cavity length can be calculated. The surrounding temperatures information is thus obtained by relating it to the cavity lengths.
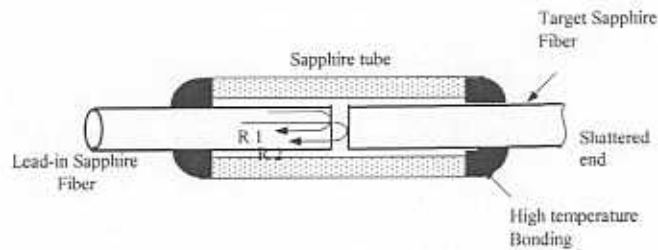
Figure 4.1. Schematic design of sapphire fiber based absolute interferometric sensor

4.1.2 Polarized-Light Interferometric Sensor (PLIS)

Polarization is a fundamental property of light, which like amplitude, frequency and phase can be used to measure physical parameters in a sensing system. The determination of the state of polarization in a system can provide information about photochemical or photo-biological or physical processes. Techniques employing polarized light are already

widely adopted in spectroscopic techniques to provide different types of information about atoms or molecules, like the electronic structure of the molecules, or orientation of the molecule.

An interference system using polarized waves will generally include a polarizing device splitting orthogonal states of polarization, located between a polarizer which sets the state of polarization at the entrance and an analyzer which makes the interfering states of polarization identical. Figure 4.2 makes the general principle of the system clear. The polarizing devices such as phase-shifters or rotators split the incident light wave into two orthogonally polarized waves. Since these waves propagate at different velocities, their phases are shifted by a quantity Φ during their propagation. After they are analyzed by a polarization states analyzer, the emerging intensity is a function of the phase shift Φ.
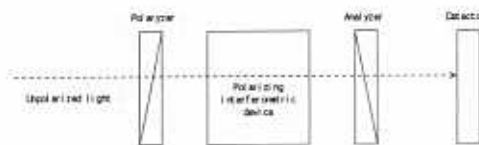
Figure 4.2. The principle of an interference device using polarized lightwaves

Due to the crystallographic arrangement of the atoms in single crystal sapphire, the material exhibits an inherent birefringence. For a wavelength of 589nm, n_o=1.768, and n_e=1.760, yielding a birefringence of 0.008. The xy plane of the index ellipsoid of single crystal sapphire is   x   n as Figure 4.3.

Figure 4.3. The XY-plane of the index ellipsoid of single crystal sapphire

35

Figure. 4.4. illustrates the working principle of the sapphire sensing head [55]. One single-crystal sapphire disk with inherent birefringence is sandwiched between a polarizer and an analyzer, whose polarization directions are parallel to each other and along z-axis direction, the principle axes (i.e.f-axis and s-axis) of sapphire disk is oriented at 45° with respect to z-axis direction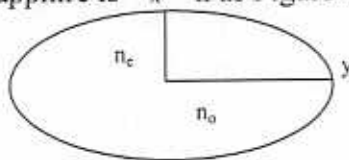. At the exit of the disk, the phases of the two orthogonal states are shifted by a quantity Φ and the emergent state of polarization is usually elliptical. In order to uncover the phase shift Φ introduced by the disk, the emerging light has to be analyzed through a polarization analyzer. The phase shift is determined by the magnitude of the birefringence and also on the relative length difference traveled by the differently polarized light. Since both the birefringence and thickness of the sapphire material are a function of temperature, the magnitude of the differential phase shift will also be temperature dependent. Therefore, by sensing the magnitude of this phase shift, the temperature can be uniquely determined.

By encoding and decoding temperature information in the phase of an optical signal, this kind of sensors design guarantees the self-calibrating capability, where that encoded temperature is not corrupted by intensity fluctuations from long term run point of view and then the better measurement repeatability than intensity-measurement based optical sensors.
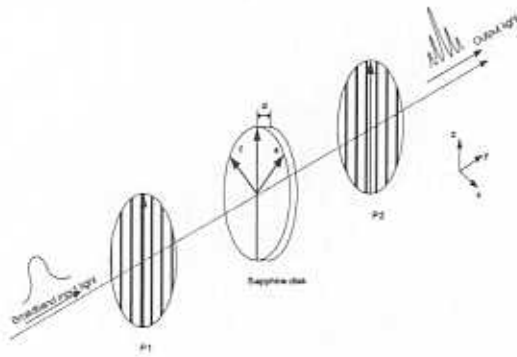
Figure. 4.4. A conceptual schematic design of sensing head; broadband polarimetric differential interferometry (BPDI)
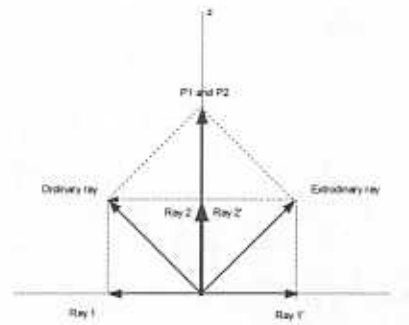
Figure. 4.5. Interfering mechanism for polarimetric differential interferometer

The optical interfering activity inside the polarimeter is shown in Figure. 4.5. Corresponding to Figure.4.4, Input broadband light is polarized by P1 and its amplitudes is A, its polarization direction, i.e. the direction of oscillation of the electric field vector, is along P1, i.e. z-direction, when this linear light propagates inside sapphire disk, the disk behaves as if it split the incident state into two linear states, having the same amplitudes, oriented along the principle axes: ordinary ray(along f-axis) and extraordinary ray(along s-axis), resulting from the 45° angle alignment between P1 and the principle axes of sapphire disk. Assuming no attenuation in sapphire disk, these two rays will propagate independently without amplitudes change, while there will be relative phase delays between them. At the end of the analyzer, only light polarized along z-direction can pass, where light is decomposed according to their polarization direction again: ordinary ray is decomposed into ray1 and ray2, extraordinary ray is decomposed into ray1' and ray2', interfering results between ray2 and ray2' will pass.

The interfering results can be expressed mathematically as following:

$$\vec{E}_{out} = \frac{1}{2}(\vec{E}_{ray2} - \vec{E}_{ray2'}) \qquad (4.2)$$

Where $\vec{E}_{out}$, $\vec{E}_{ray2}$ and $\vec{E}_{ray2'}$ are all vectors, for the output intensity

$$I = |\vec{E}_{out}|^2, \qquad (4.3)$$

It will not only depend on the magnitude of interfering electric fields, but also the phase shift Φ between those two electrical oscillation vectors:

$$
\begin{aligned}
I_{out} &= (\frac{1}{2}E_{ray2})^2 + (\frac{1}{2}E_{ray2'})^2 - \frac{1}{2}E_{ray2'}E_{ray2}\cos\Phi \\
&= \frac{1}{4}E_{ray2}^2(1 + \sin^2(\Phi/2))
\end{aligned} \qquad (4.4)
$$

where $\Phi = 2\pi d\Delta n/\lambda$. Since both d and Δn are functions of ambient temperatures, I_{out} will be temperature encoded signal, to decode the temperature values out, intensity based measurement can be done for monochromatic light, which will be described as PLIS, and spectrum measurement can be done if the input light is broadband light, which will be termed as BPDI measurement methods.

4.2 Detecting Unit

Based on both of the sensing head designs, temperature information are encoded in the interferometric signals. Three different detecting schemes are tested to decode the real-time temperature information; which are sapphire fiber extrinsic Fabry-Pérot interferometric (EFPI) sensor, intensity-measurement based polarimetric sapphire sensor

and broadband polarimetric differential interferometry (BPDI) sapphire sensor, each of them has both advantages and disadvantages.

4.2.1 SCIIB unit

As a unique signal processing method, the self-calibrated interferometric/intensity-based (SCIIB) [56] fiber optic sensor successfully combines the advantages of both the interferometric and the intensity-based fiber sensors in a single system. Through a proper design of the sensor, the SCIIB technology can provide absolute measurement of various parameters with the full self-compensation capability for the source power fluctuation and the fiber loss changes.
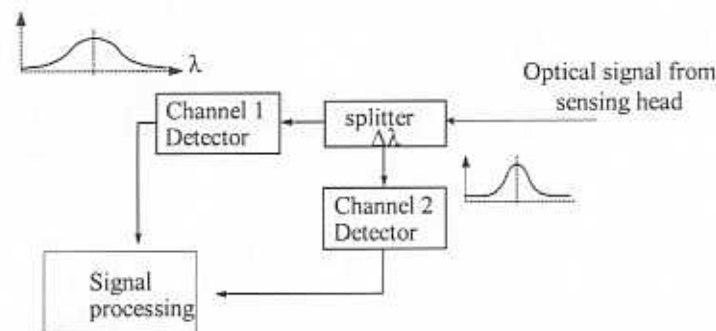
Figure 4.6. Illustration of the principle of SCIIB fiber optic sensor system

As shown in Figure 4.6, the optical signal from the sensing head is split into two channels with different optical properties through optical filtering. The light in Channel 1 remains its original spectral width (broadband spectrum) while the light in Channel 2 has a

narrower spectrum by passing it through an optical bandpass filter. The different spectral widths of the light result in different coherence lengths of these two channels. Assuming that the original spectrum width of the source can be approximated as a Gaussian profile with a spectral width of $\Delta\lambda_1$, and also assume that the spectral characteristic of the optical bandpass filter is a Gaussian profile too, but with a different spectral width of $\Delta\lambda_2$. The light spectra seen by the two SCIIB channels can thus be expressed by

$$I_{s1,s2}(\lambda) = \frac{2I_{10,20}}{\sqrt{\pi}\Delta\lambda_{1,2}} \exp\left(-\frac{(\lambda-\lambda_c)^2}{\Delta\lambda_{1,2}^{\;2}}\right), \qquad (4.5)$$

where $I_{10,20}$ are the optical powers of the two channels respectively, and λ_c is the central wavelength for both channels (here, we assume that the two channels have the same central wavelength).

The interference signals resulting from the spectra of the two channels can thus be written as

$$I_{1,2} = R \cdot \int_{-\infty}^{\infty} I_{s1,s2}(\lambda)[1 + \eta^2(1-R)^2 - 2\eta(1-R)\cos(\frac{4\pi}{\lambda}L)]d\lambda, \qquad (4.6)$$

where

- $I_{s1,s2}$ are the spectral power density distribution of the two channels respectively
- R is the reflectance at the boundary of the air and the fiber endface
- L is the cavity length

- η is the coupling coefficient of the Fabry-Perot cavity. It is a function of the cavity length L, the lateral offset, and the angular offset. Because the initial cavity length usually is chosen to be very small, the optical loss of the cavity is very small. Therefore, η can be approximated to 100%.

The reflectance at the fiber endfaces is thus about 4% of the total incident optical power. Notice that the reflectance is relatively small, the interference signals given by Equation (4.6) can thus be approximated by

$$I_{1,2} \approx 2R \cdot \int_0^\infty I_{s1,s2}(\lambda)[1 - \cos(\frac{4\pi}{\lambda}L)]d\lambda \ . \tag{4.7}$$

Equation (4.7) indicates that the interference signal is the superposition of interference contribution of all the spectral components. Here we have assumed that the photodetectors have a flat response over the source emission spectrum.

By taking the ratio of the two channels outputs, we then have the SCIIB output given by

$$s = \frac{I_2}{I_1} \approx \frac{\int_{-\infty}^\infty I_{s2}(\lambda)[1 - \cos(\frac{4\pi}{\lambda}L)]d\lambda}{\int_{-\infty}^\infty I_{s2}(\lambda)[1 - \cos(\frac{4\pi}{\lambda}L)]d\lambda} \ . \tag{4.8}$$

Figure 4.7 shows the output signals from the two SCIIB channels, and Figure 4.8 plots their ratio given by Equation (4.8) as the function of the sensor cavity length, where the source spectral width is assumed to be 40nm and that of the bandpass filter is 10nm, which corresponds to the single-mode fiber sensor case as we will discussed later.
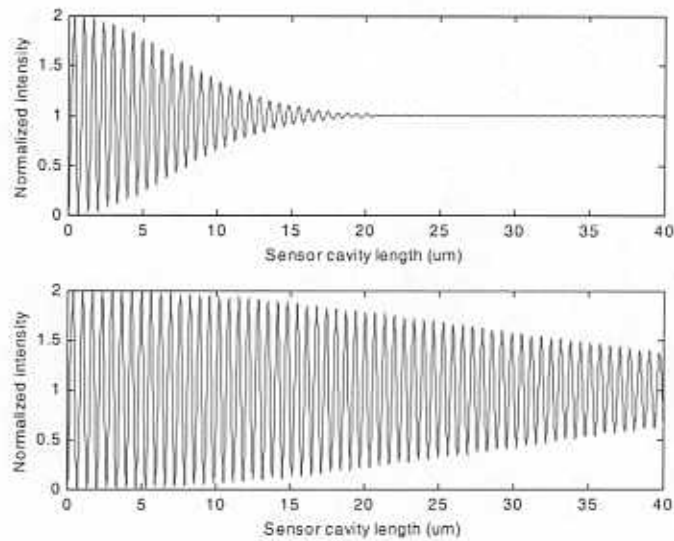
Figure 4.7. Interference fringes of the SCIIB two channels, where the source has the spectral width of 40nm and the central wavelength of 1310nm; the spectral width of the bandpass filter is 10nm, in accordance with the single-mode fiber sensor system.
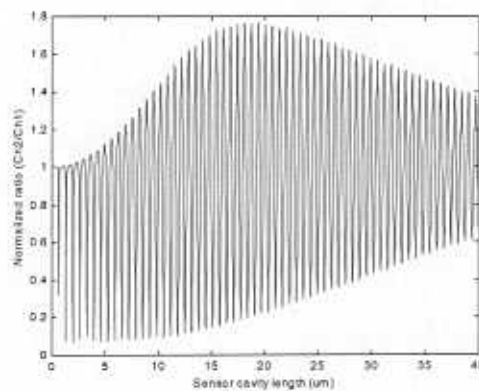
Figure 4.8. Ratio of the two channels' outputs of Figure 4.7

Regular interferometric sensors suffer from the disadvantages of sensitivity reduction and the fringe direction ambiguity when the sensor output reaches the peak or valley of an interference fringe. Sensitivity is reduced at the peak or valley of a fringe since at that point the change in optical intensity is zero for a small change in the sensor cavity length. Fringe direction ambiguity refers to the difficulty in determining from the optical intensity whether the sensor cavity is increasing or decreasing. To avoid these two problems, we design and fabricate the SCIIB sensor head to operate only over the semi-linear range of a half fringe, as shown in Figure 4.9, so that a one-to-one quantitative relation between output intensity and the sensor cavity length is obtained.

Change of sensor cavity length (um)
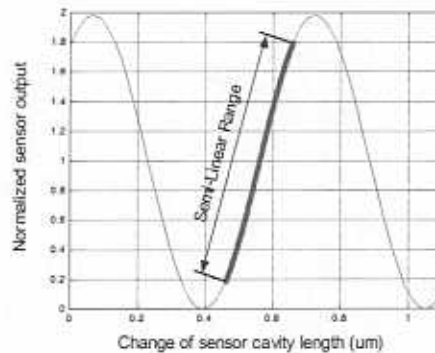
Figure 4.9. Illustration of a semi-linear operating range of fringes.

4.2.2 Intensity-measurement based polarimetric sapphire sensor

The detecting unit setup is shown in Figure 4.10. In general, the phase delay values generated by the birefringent retarder (sapphire flat) can be any positive real number, so the light output from the probe will be elliptically polarized light, A polarizing beam splitter (PBS) is used to split elliptically polarized light into two orthogonal, linearly

polarized components shown in Figure 4.11. As shown in this Figure, p-polarized light is transmitted, while s-polarized light is reflected, both with negligible absorption by the beam splitter. Two separate detectors (D1 and D2) were used to detect these two components and the detected signals are transmitted along two channels seperately. By calculate the ration of information from these two channels, self-calibration can be achieved, which eliminates the influence of the laser power fluctuation.
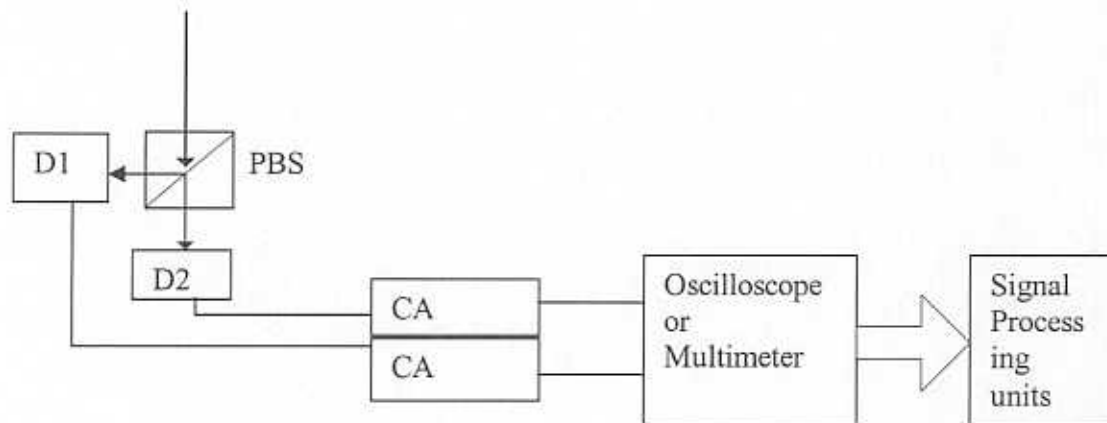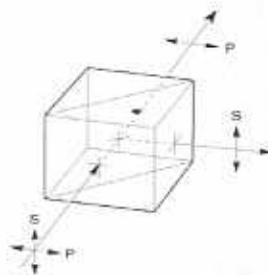

Figure 4.10. Schematic of the detection unit

Figure 4.11. Schematic of the polarizing beam splitter

The two detectors (D1 and D2) are silicon photodiodes. These semiconductor light sensors generate a current when the P-N junction in the semiconductor is illuminated by

light. Current signals from the two channels are input into the two impedance current amplifiers separately. Output signals from the amplifiers are electric voltage signals which correspond to the light intensity and are detected by simple multimeters or oscilloscopes.

Temperature decoding algorithm is based on the following mathematical model, According to the Equation (4.4) discussed in the sensing elements design section, the sapphire disk thickness d is function of temperature T:

$$d(T) = d(1 + \alpha(T - T_0)) \Rightarrow d(T) = \alpha dT + A(cons\tan t) \qquad (4.9)$$

where $A = d - \alpha dT_0$, α is thermal expansion coefficiency for sapphire material, ΔT is temperature change compared to T_0, which is room temperature 25 °C. Since $d \gg \Delta d$, also $\Delta n = n_o - n_e$ is very small (Quoted by manufacture(saphikon) approximate. 13×10^{-6} / °C), so the function between temperature and product $d\Delta n$ is linear, and temperature relation with output light intensity(polarization direction perpendicular to input linearly polarized light) will be a squared sinusoidal function of temperature T as in Equation(4.11), which is proved by our experiment results

$$
\begin{aligned}
I_{out}(T) &= I_0(1 + \sin^2(\Phi/2)) \\
&= I_0(1 + \sin^2(\pi \Delta n d(T)/\lambda)) \qquad (4.10) \\
&= I_0(1 + \sin^2((\pi \Delta n \alpha dT/\lambda) + A\pi \Delta n/\lambda))
\end{aligned}
$$

Where $A\pi \Delta n/\lambda = \phi$ is also one constant phase, so

$$I_{out} = I_0(1 + \sin^2((\pi \Delta n \alpha dT / \lambda) + \phi)) \tag{4.11}$$

Because of energy conservation, outputs of channel two will be the following:

$$I_{out-2} = I_0(1 - \sin^2((\pi \Delta n \alpha dT / \lambda) + \phi)) \tag{4.12}$$

which also contain information of temperature and input laser intensity I_0. By calculate the ratio between I_{out} and I_{out_2},

$$\frac{Iout}{Iout\_2} = \frac{1 + \sin^2((\pi \Delta n \alpha dT / \lambda) + \phi)}{1 - \sin^2((\pi \Delta n \alpha dT / \lambda) + \phi)} = R(T) \tag{4.13}$$

I_0 is eliminated thus the finial signal will only contain temperature information with immunity to optical intensity fluctuation.

4.2.3 Broadband polarimetric differential interferometry (BPDI) sapphire sensor

Intensity-measurement based polarimetric sapphire sensor simplifies Equation (4.4) by assuming d is temperature dependent only, to be accurate, both d and birefringence Δn are functions of temperature, whitelight interferometric signal processing technique directly measure the phase shift by taking all d and Δn into account without any approximation.

When illuminated by a broadband light source, the transmitted interferometric spectrum signal from the polarimeter can be expressed as:

$$I(\lambda) = 2kI_s(\lambda) \ \left(1 + \cos\left(\frac{2\pi d(T)\Delta n(T)}{\lambda}\right)\right)$$

(4.14)

Where $I_s(\lambda)$ is the spectral power distribution function of wavelength (λ) of the broadband input light source; k is a parameter describing the power loss of the optical system, and can be treated as a constant; d is the thickness of the sapphire disk; and $\Delta n = n_e - n_o$ is birefringence between ordinary ray and extraordinary ray determined by sapphire internal structure. Both d and Δn are functions of temperature T.

Ideally, the interference fringes form a perfect sinusoidal curve after it is normalized with respect to $I_s(\lambda)$ according to Equation (4.14):

$$I(\lambda) = 2k\left(1 + \cos\left(\frac{2\pi d(T)\Delta n(T)}{\lambda}\right)\right) = 2k\left(1 + \cos\left(\frac{2\pi f(T)}{\lambda}\right)\right)$$

(4.15)

where,

$$f(T) = d(T)\Delta n(T)$$

(4.16)

From the detected optical spectrum, an internally developed algorithm is employed to measure the difference of optical paths $f(T)$ between two orthogonal linearly polarized lights in the sapphire disk, which is uniquely related to the differential phase delay between two orthogonal polarized lights. The algorithm used to calculate $f(T)$ from the transmitted interferometric spectrum is described in the following secytion.

4.3. Algorithm for optical signal processing

As one of the most sensitive measurement systems, optical interferometry has been used in a variety of applications. In most of the conventional mono-wavelength interferometric systems, a coherent light source was used to achieve a large coherent length, which in turn gives out a large dynamic range. For this kind of system, the most commonly used signal demodulation method is peak counting, i.e. using a power meter to detect the intensity of the interference signal from the sensor head and an electric counter to count the total number of peaks from a reference point. Obviously, only relative measurements can be achieved by this method. Another disadvantage of this method is the lower resolution, which is about the same order as the source wavelength. Although some improved methods have been developed, it has been difficult to achieve both large dynamic range and high resolution and absolute measurement in same system.

White light or low coherence interferometry is a technique, which dates back to 1913 and was reapplied to optical fiber sensing in 1983. Instead of using a highly coherent light source, a broadband light source, such as an LED, is used. Although the power-detection approach can be used, to fully exploit the advantages of the white light system, spectrometer-based detection systems are more popular.

The white light interferometric system inherits most of the advantages from the conventional interferometer, such as immunity to the light source power drift and changing of transmission losses, high resolution, large dynamic range, etc. On the other

hand, by using the spectral domain signal processing technology, an absolute measurement of the distance between the interfering interfaces can be realized.

Considering the industrial applications, the use of a long life, low priced broadband light source (such as LED) improves the stability of the whole system and decrease of the price dramatically. Numerous applications of white light interferometric sensor systems have been reported, covering a wide range from single point measurement to distributed sensor systems.

In this research, a novel data processing method for white light interferometric system, which can improve the system resolution dramatically, is introduced. A compact white light signal-processing unit based on this algorithm has been setup, and a sub-nm resolution has been demonstrated. In addition, by using a self-compensating data processing method, high temperature stability has been achieved.

4.3.1 Existing data processing methods

Various methods have been developed to demodulate the air-gap G from the normalized interference spectrum, which is described by equation (4.15) in last section. Most of these kinds of algorithm can be categorized into two classes. The first class can achieve high resolution (which mainly depends on the resolution of spectrometer), but the dynamic range of air-gap must be limited to the half wavelength range to avoid the problem of ambiguity in signal interpretation due to the periodic nature of the signal. The second

class can achieve a large dynamic range but suffers from low resolution. The basic ideas

for these methods are introduced briefly as follow:

Class one:

Type one is based on tracing a special point in the interference spectrum (such as peak

point or valley point). Then from the wavelength of this special point, the value of air-gap

can be demodulated. The following calculation is based on peak tracing:

The wavelength λ_m of a peak point in interference spectrum satisfies

$$\frac{4\pi G}{\lambda_m} + \varphi_0 = m2\pi \qquad (4.17)$$

Where the spectral order m is a non-negative integer.

Equation (4.17) can be transformed into:

$$G = \frac{(m2\pi - \varphi_0)\lambda_m}{4\pi} = \frac{K_m}{2}\lambda_m$$
$$\qquad (4.18)$$
$$K_m = \frac{(2m\pi - \varphi_0)}{4\pi} = m - \frac{\varphi_0}{2\pi}$$

Obviously, for a given peak point, the value of K_m is a constant.

To demodulate the air-gap G from a special peak wavelength λ_m, K_m must be acquired

first. The identification of the interference order m is so difficult that the unambiguous

operating range of the air-gap is limited in only half of the source wavelength.

The resolution of the measurement is mainly dependent on the resolution of spectrometer.

From equation (4.18), the relative error of this system induced by the spectrometer can be

described as

$$\left|\frac{\Delta G}{G}\right| \cong \left|\frac{\Delta \lambda}{\lambda}\right| \quad (4.19)$$

Class Two:

To realize absolute measurement in a large range, at least two special points in the interference spectrum need to be used. Suppose λ_1 and λ_2 ($\lambda_1 > \lambda_2$) are the wavelengths of two adjacent peak points in the interference spectrum, their interference orders are m and $m+1$.

From equation (4.17),

$$4\pi G/\lambda_1 + \varphi_0 = m2\pi \, ;$$

$$4\pi G/\lambda_2 + \varphi_0 = (m+1)2\pi$$

The air-gap G can be demodulated from:

$$G = \frac{\lambda_1 \cdot \lambda_2}{2(\lambda_1 - \lambda_2)} \quad (4.20)$$

Obviously, this method overcomes the ambiguity problem of class one. The dynamic range is only limited by the coherence length of the white light system.

From equation (4.19), the relative error induced by the spectrometer is

$$\left|\frac{\Delta G}{G}\right| \cong \sqrt{2}\left|\frac{\lambda_2}{\lambda_1 - \lambda_2}\right| \bullet \left|\frac{\Delta \lambda_1}{\lambda_1}\right| \quad (4.21)$$

Comparing equation (4.19) with equation (4.21), in class two type signal processing algorithm, the relative error induced by the spectrometer will be enlarged by a factor of $\sqrt{2}|\lambda_2/(\lambda_1 - \lambda_2)|$. In our system, the central wavelength of the light source (LED) is 850nm. In the normal operating range (air-gap 5-15 μm), this factor is about 15—50,

which means the resolution of type two is much lower than class one signal processing techniques.

4.3.2 New Algorithm

To combine the advantages of these two kinds of methods together, we developed a novel data processing method, which can realize both high resolution and a large dynamic range simultaneously.

The basic idea of this method is: use wavelengths of two adjacent peak points in the interference spectrum to get a rough air-gap value from equation (4.17) (large dynamic range is achieved); this rough air gap value will be used to determine the order number m and a rough K_m' value for one of the two peak points (equation (4.18)). Then, by using a calibrated K stored in the computer, an accurate K_m can be recovered from the rough K_m'; Using equation (4.18) again, the accurate air gap value can be calculated from the accurate K_m and the peak wavelength (therefore, high resolution is achieved).

The technique used here to recover the accurate K_m from the rough K_m' value is presented as follows:

In equation (4.18), although K_m is not an integer, for a given peak, it is a constant. And for adjacent peaks, the difference in K_m is 1. For example, if the K_m of one peak is 12.34, then, for the other peaks, the K_m will be 13.34, 14.34, 15.34...and 11.34, 10.34, 9.34... and so on.

By calibration, the K_m value for a special peak (K_m^0) can be acquired and stored in the computer. During the process of measurement, when the rough K_m' value for the peak has been acquired, although we don't know the order m of this peak point, the difference between K_m and the stored K_m^0 should be a integral number. So, the accurate K_m can be calculated by adding K_m^0 with the integer part in the difference between the rough K_m and K_m^0.

$$K_m = K_m^0 + INT(K_m' - K_m^0 + 0.5) \qquad (4.22)$$

Where, function INT (...) means to obtain the integral part.

Another approach for recovering the accurate K_m value from the rough K_m' value is: calibrate K_m for all the peak points that will be used in the whole dynamic range and store them in the computer; during the process of measurement, when a rough K_m' value is acquired, the closest K_m stored in the computer will be chosen as the accurate K_m.

Both approaches have been realized in the Visual Basic environment, with the second one producing a more robust performance. The experimental results are presented in the following section.

4.4 Supportingsignal processing units

Combining the sensing elements and detecting units, the basic temperature measurement system can then be constructed. To ensure the whole system functioning for the whole proposed temperature measurement range with the certain sensitivity and accuracy, some

supporting units are necessary, which include both electrical hardwares and computer softwares.

One problem for the sensing system is how reduce the influence of blackbody radiation on the measurement results. The proposed temperature measurement is over 1500 °C, for this high temperature measurement, the optical intensity from blackbody radiation background will becoming more influential on the designed temperature measurement system. Since the temperature information is decoded from the light from LED in the sensing system, all the background blackbody radiation is superimposed on the desired LED output light, it is totally undesired and treated as noise. At low temperatures, the effect of the blackbody radiation is negligible, while those noise is most influential at temperatures over 1000 °C, due to the increasing strength of the blackbody radiation as a function of temperature. One supporting subsystem is then designed to deal with blackbody radiation reduction.

Another supporting unit is a temperature acquiring subsystem, which is based on thermocouple for temperature referencing.

4.4.1 Blackbody radiation background

If a cavity with perfectly absorbing (i.e. black) walls is maintained at a fixed temperature T, its interior will be filled with radiant energy of all wavelengths, this radiation is referred to as blackbody radiation. Since the designed temperature sensing system will be

applied to high temperature environment up to 1600°C, blackbody radiation will become strong to affect optical signal emitted from LED.

If blackbody radiations are in equilibrium, both within the cavity and with its walls, then the rate at which energy is radiated across any surface or unit area is independent of the position and orientation of that surface, the radiation intensity is specified by a distribution function K_λ, such that K_λ is given by $\int_0^\infty K_\lambda d\lambda$ and $K_\lambda d\lambda$ is the intensity due to radiation with wavelength between λ and $\lambda + d\lambda$. K_λ is a universal function, dependent only on temperature and wavelength, not on the size or shape of the cavity or on the material of its wall.

$$K_\lambda = \frac{C_1 \lambda^{-5}}{e^{C_2/\lambda T} - 1} \tag{4.18}$$

It is called Planck Formula in blackbody radiation, where $C_1 = 1.19089*10^{\wedge}(-16)$, $C_2 = 0.0143883$ [24], some high temperature sensing systems employ this formula to detect temperature values. Figure 4.12 and Figure 4.13 show blackbody radiation intensity distribution curve with different wavelengths and temperatures.
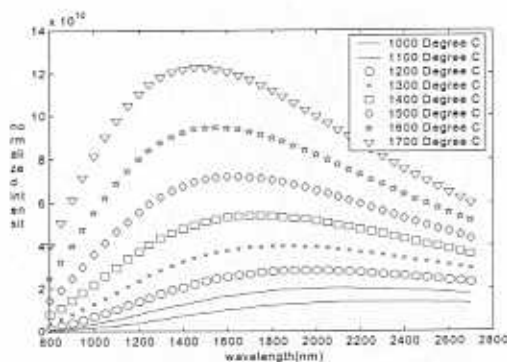

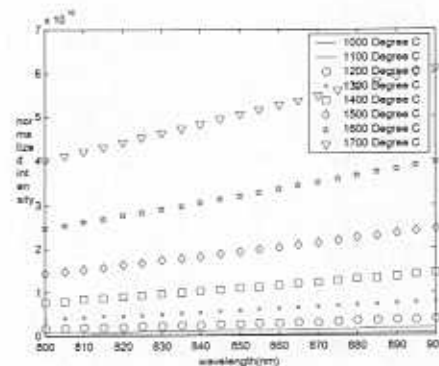**Figure4.12**. Theoretical results of blackbody radiation at different temperatures

Figure4.13. Theoretical results of blackbody radiation at different temperatures, for the interested wavelength range(800nm~900nm)

The blackbody radiation background will be superimposed on the LED interference, and will be detected by the spectrometer. As shown in Figure 4.14, at 1297^0C , the interference fringes from the BPDI system is shifted up compared to the measurement results at low temperature because of blackbody radiation increasing. It will greatly degrade the validity of approximation of sinusoidal function shown in Equation (4.15), as shown in Figure4.15, it is can not be approximated as sinusoidal function again, Equation (4.17) is thus not valid for the calculation of thickness of saphhire flat. More detailed analysis between blackbody radiation and interference fringes from LED light source are shown in Figure 4.16.
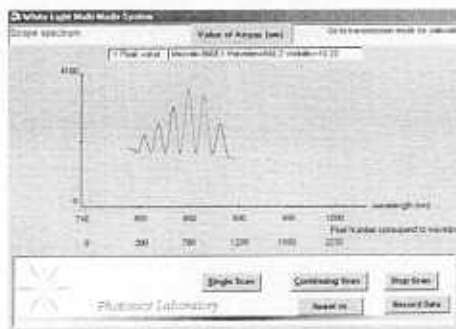
Figure4.14. At 1297^0C, interference fringes from BPDI sensing system.
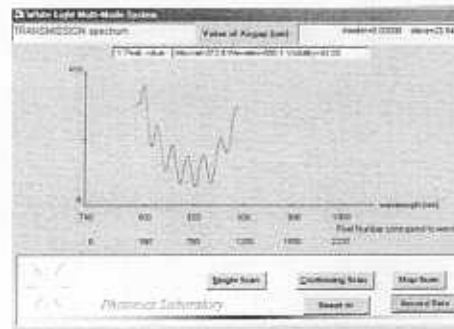
Figure 4.15. At 1297^0C, Normalized interference fringes from BPDI system according to Figure 4.14.

(a)   (b)
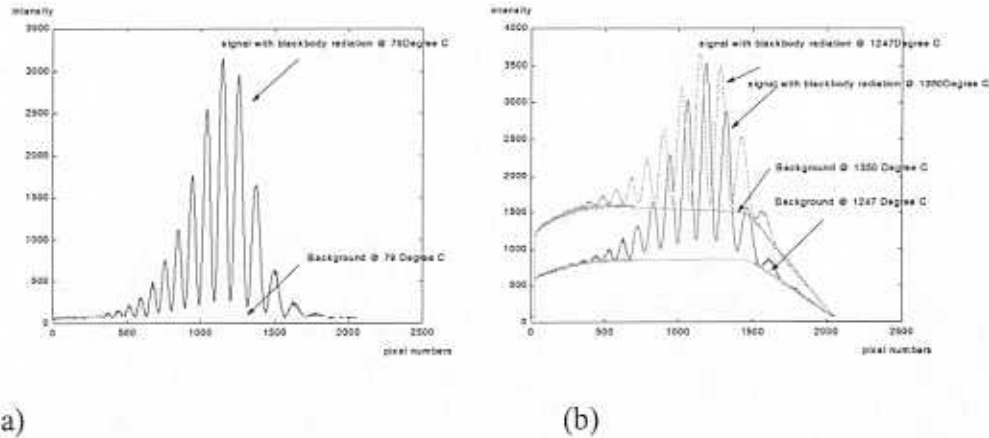
Figure4.16, Relation between blackbody radiation and interference fringes at different temperatures.

One method to reduce the blackbody radiation is to modulate the LED output light with a certain frequency FM signal, at the detection unit part, a band pass digital signal filter [57] (IIR filter, Infinite-Impulse Response filter) is employed to filter out the desired optical signal from LED only, background from blackbody radiation will be blocked as a DC component in the detected signals. The frequency used for LED modulation is 3Hz, the designed filter is shown in Figure 4.17, whose pass band is from 2Hz to 5Hz. The inteferogram is shown in Figure 4.18.
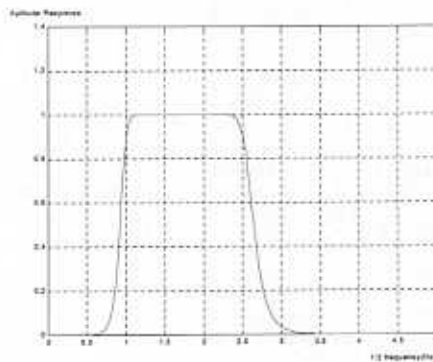
Figure 4.17. Amplitude response of IIR filter.
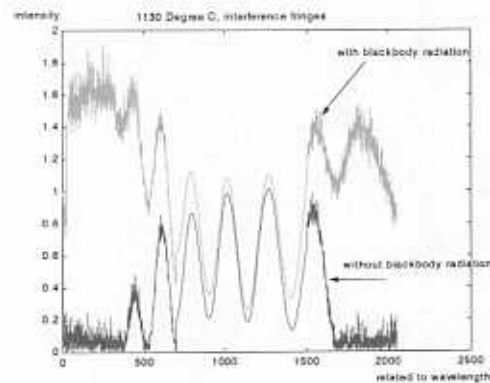
Figure 4.18. Interference curve with blackbody radiation subtraction.

4.4.2 Temperature acquisition system

Before calibration work on the designed temperature measurement system, all experimental results are relations between optical path differences vs. time, which is indirectly related to real time temperature values. A temperature-acquiring subsystem is needed to obtain real-time temperature values for calibration purpose, which provides the relation between optical path differences and temperatures for the sensing system.

In this subsystem, real time temperature values from B type thermocouple are displayed in the temperature monitor and then acquired by a computer using RS232 interface, as shown in Figure 4.19. In computer, the temperature value will then be one to one related to the optical path differences in the sapphire disk by software communication between temperature acquiring subsystem and optical path differences measurement and calculation subsystem.
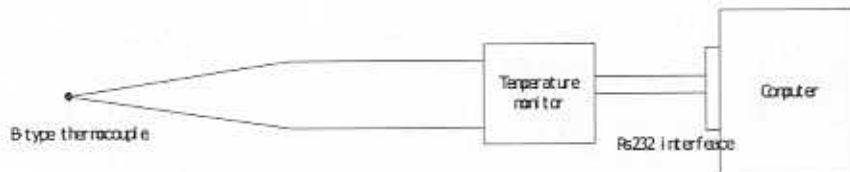

Figure 4.19. Temperature acquisition subsystem for calibration purpose

One DPi32-C24 temperature meter from Omega® is used to acquire temperature values

from B-type thermocouple, its RS-232 serial digital communication port is used to communicated with computer directly. By employing Visual_Basic, a graphical user interface (GUI) is designed to display the real-time temperature values; each of these values is uniquely corresponding to one gap value, these gap values are difference between two orthogonal linear polarized lights propagating path in the sensing element, as shown in Figure 4.20, the gap value is 20.10391 micrometer at temperature 1181.0 °C.

With this temperature acquirement subsystem, the performance of the designed temperature sensing system, such as repeatability, accuracy compared to thermocouple and temperature resolution and etc, can be evaluated in detail.
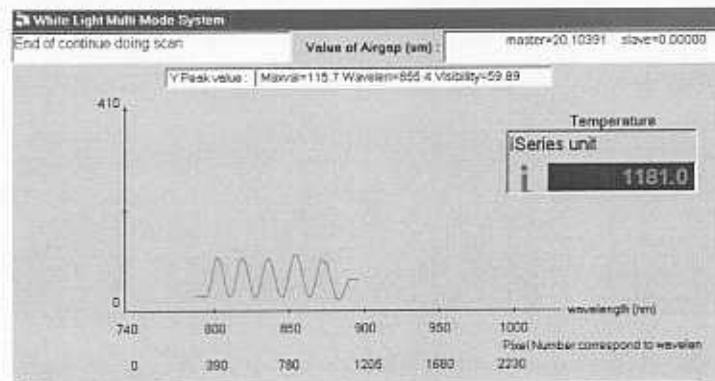
Figure 4.20. Real time temperature is related to gap values

Chapter 5. Experimental results

By employing the two working principles of optical sensing elements and three detecting schemes presented in previous chapter, five different temperature measurement systems based on optical interference metrology can be constructed as shown in the Figure 5.1.
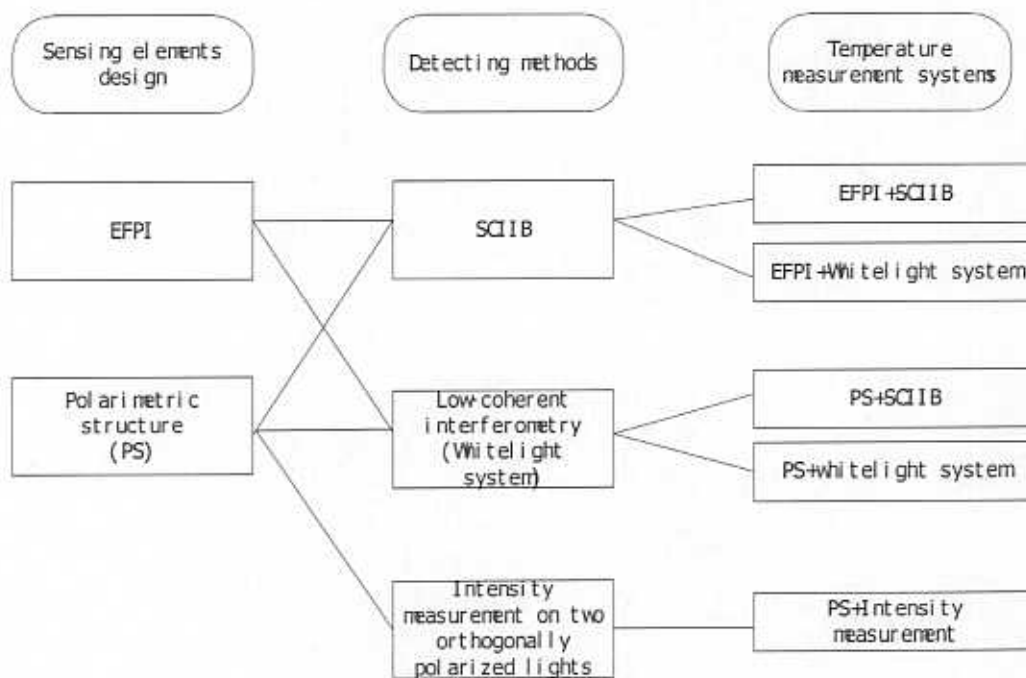

Figure 5.1. Temperature measurement systems based on designed sensing elements and detecting units

In this chapter preliminary testing results are summarized from three different temperature measurement systems: EFPI+whitelight; PS+whitelight system; PS+intensity measurement, named as sapphire fiber extrinsic Fabry-Pérot interferometric (EFPI) sensor, intensity-measurement based polarimetric sapphire sensor and broadband polarimetric differential interferometry (BPDI) sapphire sensor separately, which are presented in the order of research carrying-on processes. Based on these preliminary

results, the PS+whitelight system, also called broadband polarimetric differential interferometry (BPDI) was chosen as an optimal approach for high temperature measurement in coal gasification systems for further prototype instrumentation development.

5.1 Sapphire fiber extrinsic Fabry-Pérot interferometric (EFPI) sensor

5.1.1 system setup

The schematic configuration of the sapphire-fiber-based extrinsic interferometric sensor is shown in Figure 5.2. The light from the broadband source (LED) is coupled into a silica fiber. A 3dB coupler is used in the system to inject light into the optical fiber and also direct the interference signal from the sensor head to the detector. An anti-reflection silica-to-sapphire fiber connector is used to transmit light from the silica fiber to the sapphire fiber. A sapphire air gapped EFPI sensor head is formed by inserting the lead-in single crystal sapphire fiber into the one end of the sapphire tube and inserting a short piece of sapphire fiber into the other end of the tube to act as the reflecting surface (target fiber). Both the lead-in and the target sapphire fiber ends are polished to optical quality. While one end of the target sapphire fiber is highly polished, the other end is shattered to prevent any significant reflection that would interfere with the measurements. The light propagating in the lead-in sapphire fiber is partly reflected (7%) at the first sapphire-air boundary. The transmitted light travels through the air gap and is also partially reflected (7%) at the end face of the target sapphire fiber. An interference signal is generated by

these two reflected waves and the phase difference depends on the length of the air gap. The interference signal is processed in a computer-interfaced spectrometer so that the absolute cavity length can be measured.
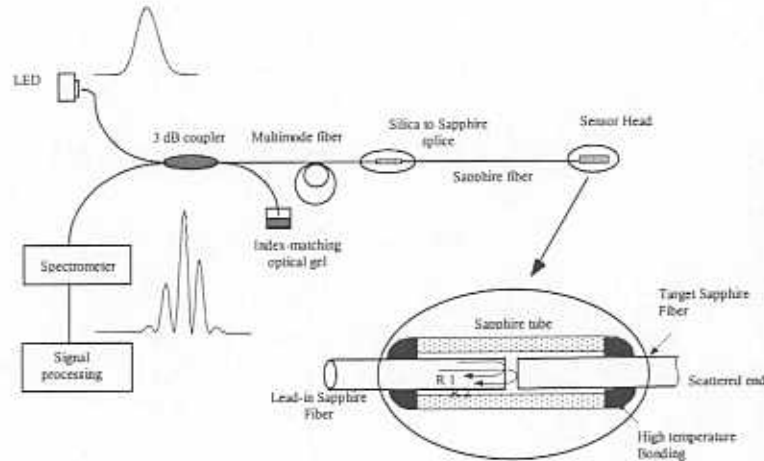

Figure 5.2. Schematic design of sapphire fiber based absolute interferometric sensor

5.1.2 Experimental results

One 100μm diameter sapphire fiber without cladding is used to construct the EFPI sensing element; an LED with a central frequency λ_0 of 850 nm and a spectral width $\Delta\lambda$ of 80nm (its a spectrum shown in Figure 5.3) is the light source in the experiments. Figure 5.4 shows the output interference spectrum of the sapphire EFPI sensor with a cavity length of 6.5μm. Figure 5.5 shows the output spectrum with a cavity length of 21.8μm. As seen in these two figures, when the cavity length increases, the visibility decreases significantly, the measurable cavity length thus are limited to certain ranges.

The sensor was placed into an electrical heated oven, the temperature was increased from room temperature to 950°C. The data were recorded at steps of 20°C as shown in Figure 5.6. The fluctuation which was seen was suspected to be the unstable heating conditions of the oven during the rapid heating.

5.1.3 Discussion

Because of the huge numerical aperture (about 1.64) of the sapphire fiber, very weak interference signal can be generated in the cavity formed by two sapphire fibers, also the inter-mode dispersion in the transmission multimode sapphire fiber degrades the interference fringes generated outside the fiber, thus it is hard and very time–consuming to fabricate sapphire EFPI sensing elements, and almost impossible to be deployed in really industry environments, where outside vibration can excite all of the multimodes in the sapphire fiber, which may totally destroy the interference fringes from the fiber gap.
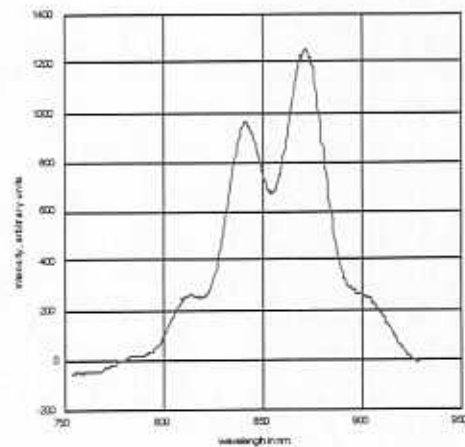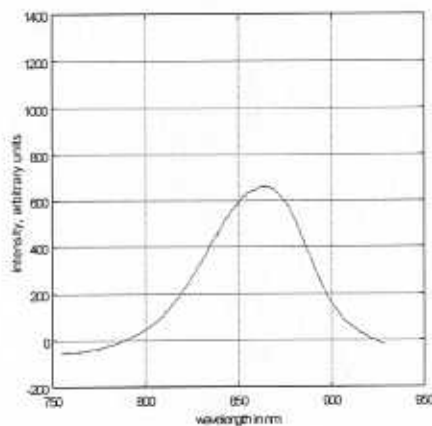
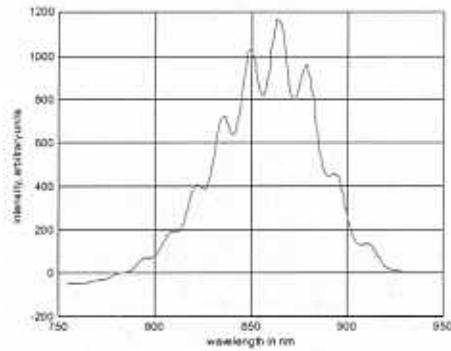Figure 5.3. Output spectrum of λ_{center}=850nm LED. Figure 5.4. Output spectrum with L=6.5μm

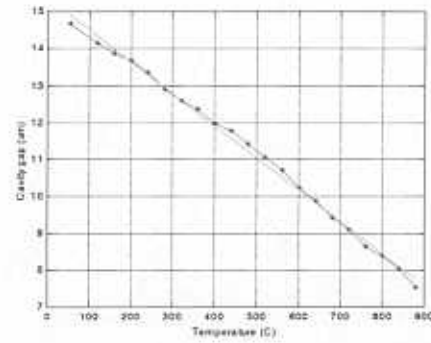**Figure 5.5**. Output spectrum with L=21.8μm

Figure 5.6. Air gap change versus temperature for single crystal sapphire sensor

5.2 Intensity-measurement based polarimetric sapphire sensor
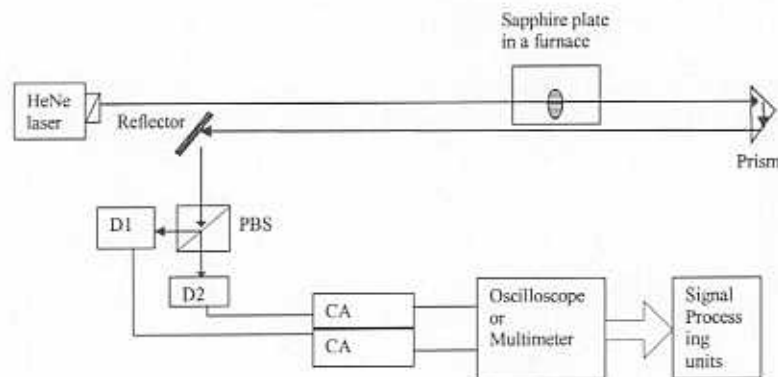

Figure 5.7. Schematic design of intensity-measurement based polarimetric sapphire sensor

5.2.1 System setup

As shown in Figure 5.7, the PS is formed by the output mirror of HeNe laser, which is a brewster window, i.e a polarizer for HeNe light, and a PBS as an analyzer; intensity measurement subsystem is composed of Detector 1 and 2, together with current amplifiers, oscilloscope and signal processing units.

The furnace used for this set of experiments was a Thermolyne box type front-loading 1200°C maximum temperature capability furnace. A K-type (chromel-alumel) thermocouple was used to monitor the temperature immediately adjacent to the single crystal sapphire plate. the single crystal sapphire plate was placed in a piece of low-density, alumino-silicate refractory brick. A slot with the width of the sapphire plate was cut into the refractory brick to hold the specimen during heating. In this manner, no refractory cement had to be used which could influence the measurement results. The thermocouple was placed close to the specimen. A hole was drilled from the back of the furnace. A similar size hole was aligned and drilled through the front of the furnace such that the laser beam directed through the hole in the rear of the furnace would pass through the single crystal sapphire plate and exit the front of the furnace unobstructed. The system with the door closed and the laser beam in operation is shown in Figure 5.8. The laser beam can be clearly seen exiting the furnace, being reflected at the 45/45 prism and contacting the detected heads.

The helium neon laser (wavelength $\lambda = 632.8nm$) is used directly as the light source. The output from the laser is already linearly polarized because the output mirror in the laser cavity is tilted by an angle corresponding to the Brewster angle. One of the sapphire flat's optical principal axes (X axis or Y axis) is aligned at $45°$ relative to the light polarization direction, i.e. $\theta = 45°$. By using PBS, the two orthogonal components of the output light are separated into two directions and measured individually. During the testing process, the temperature was either increased from room temperature ($25°C$) to $1200°C$, which was the temperature maximum of the furnace used, or cooling down from $1200°C$ to room temperature. In all experiments, the temperature was also measured by using a thermocouple (K type).

Figure 5.8   Figure 5.9

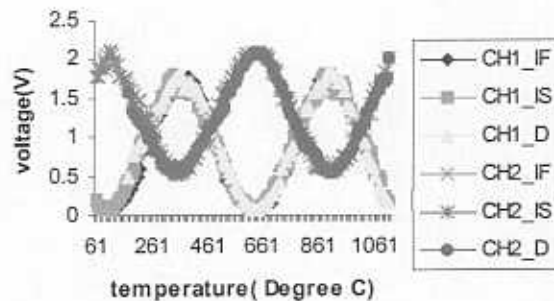Figure 5.8 . Photograph of the experimental setup in operation during testing

Figure 5.9. Experimental results of the temperature sensing system. CH1_IF: Channel1 signal for increasing temperature faster; CH1_IS: Channel1 signal for increasing temperature slower; CH1_D: Channel1 signal for decreasing temperature; CH2_IF: Channel2 signal for increasing temperature faster; CH2_IS: Channel2 signal for increasing temperature slower; CH2_D: Channel2 signal for decreasing temperature.

5.2.2 Experimental results

The sapphire flat used in the setup was a disk, with thickness d=1.05mm, diameter $\Phi = 25.36mm$. The detectors used were silicon photodiodes (from UDT). The impedance amplifiers (from Oriel) were used to transform the current signal into a voltage signal with a gain of 10^4(V/A). Two multimeters were used to measure the voltage signals. Typical experimental results are shown in Figure 5.9.

5.2.3 Discussion

Based on the theoretical analysis in Section 4.2.2, Equation (4.11) predicts that the voltage signals should be a squared sinusoidal function of temperature, which is clearly the result obtained as shown in Figure 5.9. Due to the thickness of the sapphire disk we used, there were approximately two periods shown for the temperature change in the range from 61°C to 1111°C.

To evaluate the temperature measurement results, as shown in Figure 5.9 (a) channel 1, and Equation (4.11) is simplified into Equation (5.1) which resulted in the relation that the light intensity is a squared sinusoidal function of temperature. The temperature can be obtained by solving Equation (5.1):

$$I_{out} = I_0 \sin^2 ((\pi \Delta n \alpha dT / \lambda) + \Phi)) = I_0 \sin^2 (BT + C) \qquad (5.1)$$

where B and C are approximated as constant numbers. By putting I_{out} numbers into Equation (5.1), I_0, B and C are determined, then T can be calculated individually by each I_{out}. The fitting curve and original data is shown in Figure5.10, the fitting curve function is:
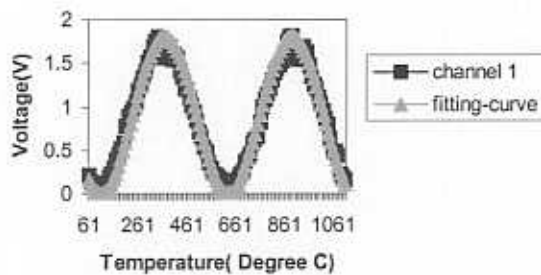
$$I_{out} = 1.81\sin^2(0.006T - 0.6672) \qquad (5.2)$$

Figure 5.10. Squared sinusoidal function curve fit of channel one data
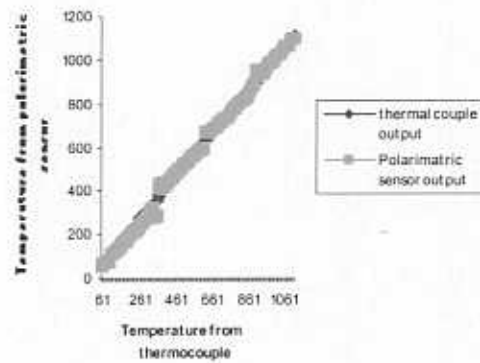
Figure 5.11. Polarimetric sensor results as compared with thermocouple results

Based on the data from channel 1, and by inversing Equation (5.2), the temperature results from the polarimetric sensor system can be calculated. The results of this operation are plotted in Figure 5.11 to be compared with the thermocouple output. Figure 5.12 shows the difference between the thermal couple output and the polarimetric sensor output. We can see that a relatively large difference occurs at the peak and valley regions of the squared sinusoidal function, which is remarkably affected by the multi-beam interference, which will be discussed in the following paragraph. For the testing temperature range, most of the difference is under 30 °C, and at higher temperature, the differences are even smaller for this fitting curve.
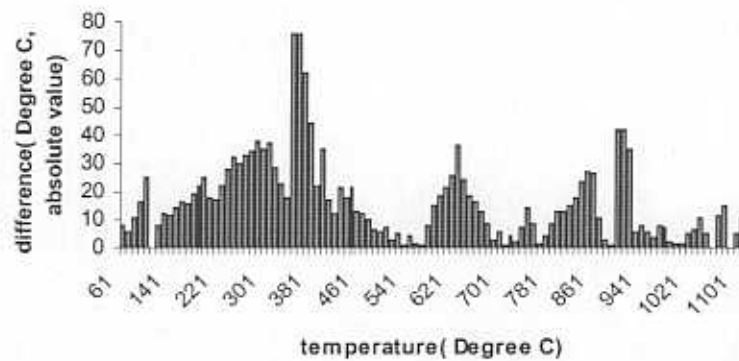
Figure 5.12. **Difference between thermocouple results and polarimetric sensor results**

Some ripples along the curves are shown in Figure 5.9, those ripples are easier to observed at the peaks and valleys of the sinusoidal curves. These are caused by the multi-beam interference, also called etalon effect, which is the oscillations resulting from constructive and destructive interference of light waves bouncing back and forth between the two well polished parallel surfaces of the optical windows. To test this phenomena, the disk is aligned with one of its principle axis, for example the X axis, parallel to polarized direction of input linear polarization light, thus the polarization light interference is therefore eliminated by no light transmitting along Y axis.
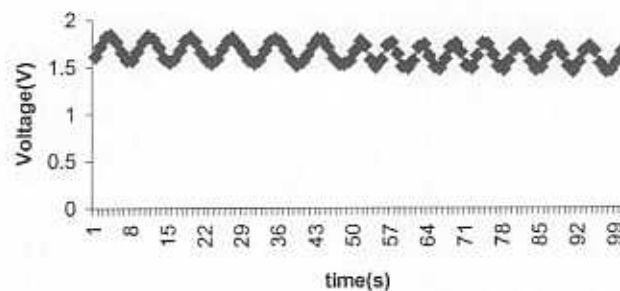

Figure 5.13. Voltage signal vs. time during temperature increasing process

A computer recorded results in Figure 5.13, the data are plotted as a function of time instead of temperature. Those data were collected every 10 seconds as the furnace was heated from 790 °C to 1200 °C. Since the effect of the polarized light interference is eliminated, the optical intensity is periodically changed by the etalon effect when the disk thickness changes. The multi-beam interference always exists for both channels as long as the coherent length condition is met by the disk thickness. Because of the relatively low reflectivity of the sapphire disc surface, the multi-beam interference fringes is about one order of magnitude less than the polarization light interference. In the peak and valley regions of the sinusoidal curves, this interference fringes from etalon effect can be observed easily, while in the other regions it is swamped by the polarization interference fringes.

5.2.4 Improved design

For the selected sapphire sensing element thickness, the response of the polarimetric sensor is a periodic function, ambiguities are generated between the measured voltages and the temperature values. Reducing the thickness of the sapphire sensing element to certain values may fix one quarter of the sinusoidal response curve to the proposed temperature measurement range, thus the measured voltage values can be calibrated to temperatures by a one-to one relation. Not only determining the temperature measurement range coresponding to the part of response curve (squared sinusoidal function), the thickness selection will also affect the polarimetric sensor initial working point, the best way to select the right sensing element thickness is to do experiments.

For the undesired etalon effect, by polishing a certain angle between two surfaces of the sapphire disk, it can be minimized or eliminated. As an alternative method, since the etalon interference fringes are a function of temperature, new mathematical model taking the etalon effect into account and precise calibration between voltage signal output and temperature of the system may eliminate the need for precise angle polishing of the sapphire plate. By taking the etalon effect into account, the large deviations between the thermocouple and the optical sensor at the peaks and valleys, , will be greatly reduced because of the multibeam interference effects. This means the accuracy of the polarimetric sensor will be increased relative to the thermocouple. Another way to eliminate the etalon effect is to choose the right light source with smaller coherent length than the sapphire disk thickness, thus there will be no interferences from the internal oscillating light of the sapphire disk.

5.3 Broadband polarimetric differential interferometry (BPDI) sapphire sensor.

5.3.1 System setup

For a coal gasifier, it is not practical to use a system which operates in transmission mode setup for the polarimetric sensing structure, where two fiber collimators at two opposite sides of the refractory wall are needed. A reflection mode polarimetric sensing structure setup is designed instead of transmission mode setup, as shown in Figure 5.14, where only one fiber collimator is used, it works to collimate input light and also collect light

reflected back from a 45-45-90 degree prism after the sapphire sensing disk. This prototype sensor is fabricated as total sensing tube length about 2 meters, with diameter 3.5cm, which consists sapphire protection tube and extension tube (round single bore cast alumina 99.8% tube). Sensing element (a sapphire disk) is located in the protection tube which will be put into high temperature furnace, while at relatively low temperature end, both optical polarizer and optical fiber collimator are inserted into the tube. Since one 45-45-90 degree prism is used to reflect light back from the end of sensing tube, only one optical polarizer is used to work both as polarizer for the input light and polarization analyzer for the reflected light, which not only reduces the cost, but also simplifies the tube assembly. The total sensing tube is integrated as one fixed long tube, which makes it robust enough to survive harsh environment.
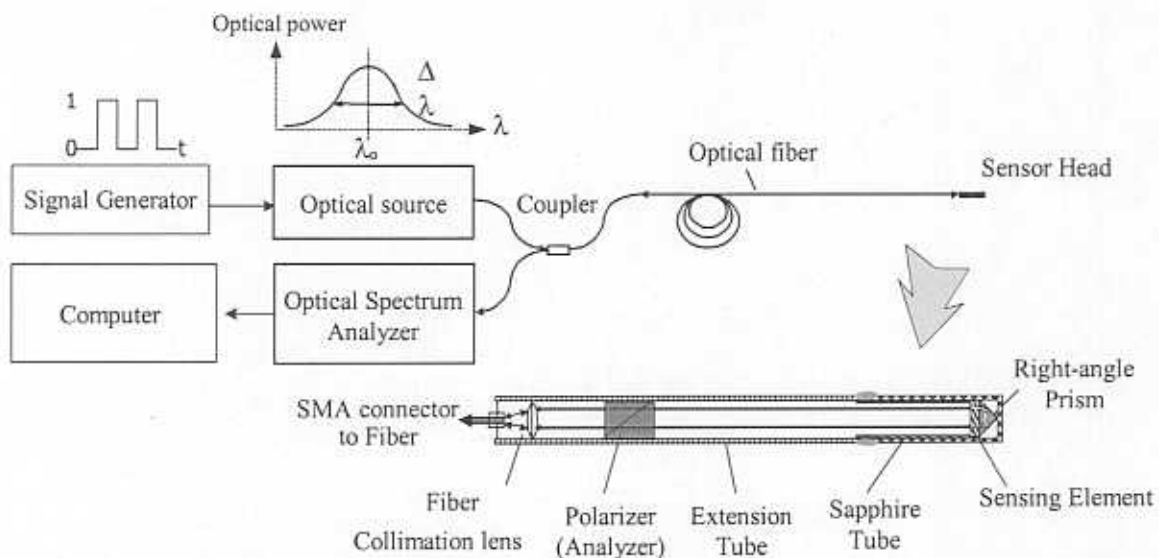
Figure 5.14. Schematic design of BPDI based optical single crystal sapphire high temperature measurement instrument.

Photograph of zirconia prism and sensing elements (sapphire disk) is shown in Figure 5.15, and Figure 5.16 shows sapphire tubes: inner sapphire tube is used to support

sensing element and zirconia prism, outer tube is used for protection. And Figure 5.17 is part of sensing head, it assembles all tubes, sensing element and zirconia prism together and to be put in the location where temperature measurement is needed. Based on the materials properties, this assembly can survive chemically corrosive high temperature environment in the coal gasifier.

Figure 5.14. shows the schematic design of BPDI based optical single crystal sapphire high temperature measurement instrument. Optical signal from a broadband LED (centered at 850nm, wavelength ranges from 810~890nm) is injected one 2.0m lead-in multimode optical fiber cable and propagates to the sensor tube, the light coming out from fiber is collimated by a collimator and then pass through the polarizer, after the polarizer, the light becomes linearly polarized and is incident into the sensing elements perpendicularly, since one 45-45-90 degree prism is behind the sensing elements, light will be reflected right back, and passing through polarization analyzer, then be collimated into fiber and conducted into a fiber optic PC plug-in spectrometer (PC2000 from Ocean Optics, Inc.), which is composed of a grating and CCD array, the intensities of the spectral components of the signal are measured by the CCD array and further signal processing, such as signal demodulation and gap calculation, will be done in the computer. An Omga type B high-temperature thermocouple (0.15'' diameter, 6%RH-Pt, resolution 0.5 °C under 1000 °C and 1.0 °C above 1000 °C) was used as the temperature monitor; the sensor was heated in one high temperature furnace. Figure 5.18 shows the sensing system from different view angles.
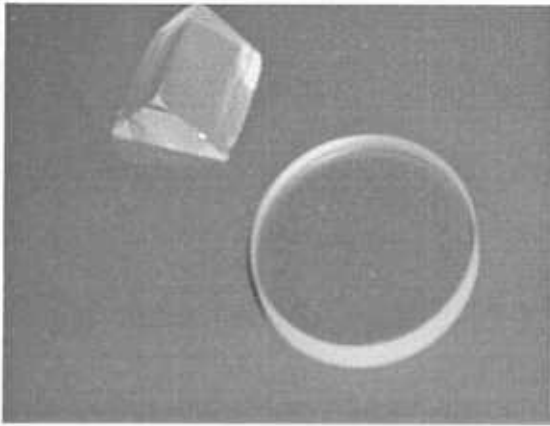
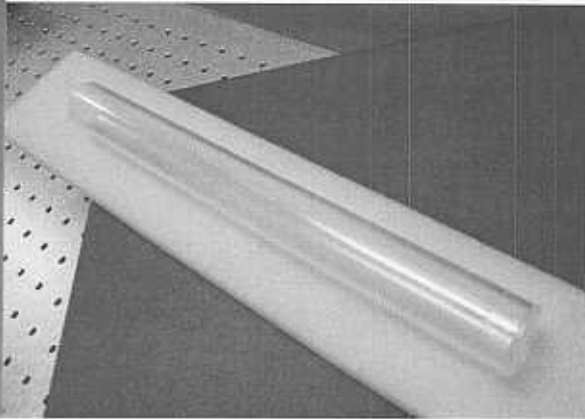Figure 5.15 Zirconia prism and sapphire disk

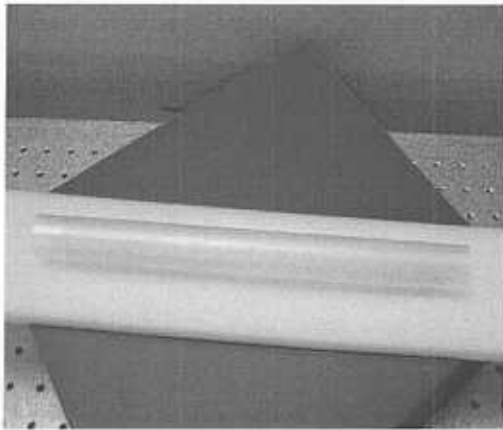Figure 5.16 (a) Single crystal sapphire outer tube

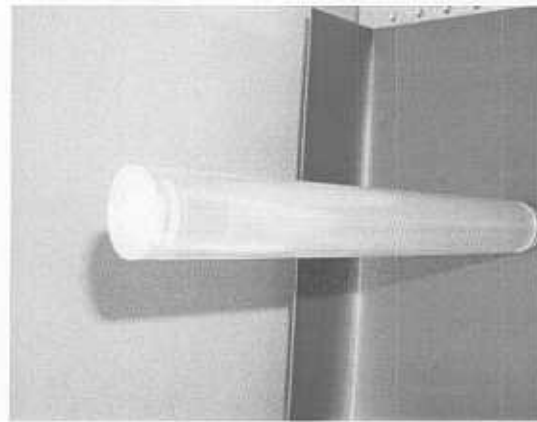Figure 5.16 (b) Single crystal sapphire inner tube

Figure 5.17 Prism, disk and tubes assembled

Figure 5.18(a) Overview of the sensing system. Figure 5.18(b) Sensing head in the high temperature
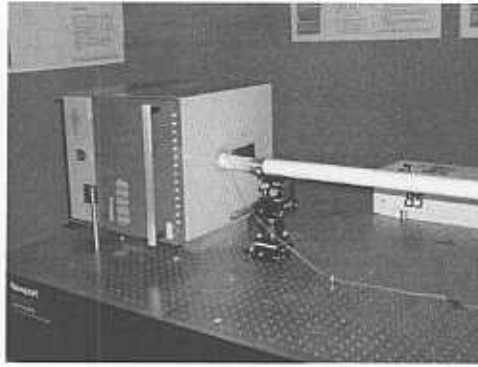
furnace

Figure 5.18(c) Sensing head is heated up over 1000 °C

Figure 5.18. Sensing system setups

5.3.2 Initial Experimental results

Figure 5.19 shows one experimental curve between gap values and time, which is a temperature decreasing process from 1050 ^{0}C to 347 ^{0}C, where gap values are uniquely related to time, which corresponds one unique temperature values, then gap values can be related to temperatures by one-to-one calibration. The experimental results basically prove that the designed sensor system works for the measured temperature range, i.e. below 1050 °C. With the same system design to measure higher temperatures, results are shown in Figure 5.20 for temperature upto 1375 °C, some unstable data appear over high temperature region, those data break the one-to-one relation between gap values and temperatures, which means further improvements on current system design are needed to measure temperature as high as 1500°C as proposed.
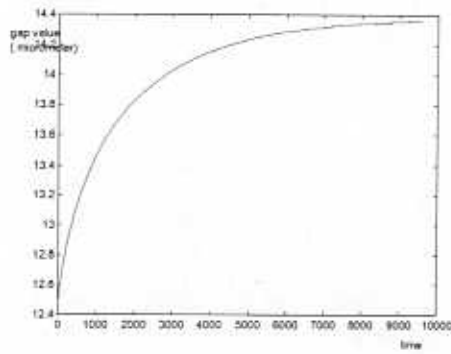
Figure 5.19. Results from BPDI system for temperature decreasing from 1050 ^{0}C to 347 ^{0}C
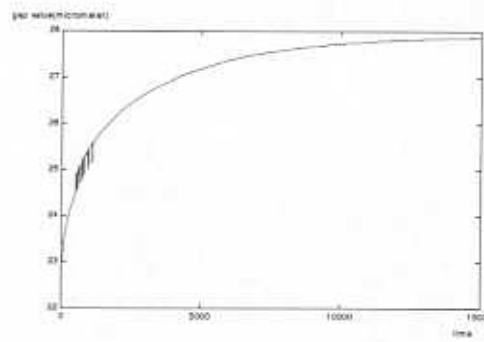
Figure 5.20. Results from BPDI system for temperature decreasing from 1375 ^{0}C to 79°C

5.3.3 Blackbody radiation reduction in BPDI

As discussed in last chapter, blackbody radiation is the main factor that degrades performance of BPDI system. Without subtraction of blackbody radiation, the system can measure temperature up to 1050°C, shown in Figure5.19. Figure 4.11 shows that blackbody radiation intensity increase with temperature increase. For temperature higher than 1050 °C measurement, smooth curves, which represent one-to-one relation between gap values and temperatures, cannot be achieved. Figure 5.20 shows typical results.

Several digital processing methods are tried to reduce blackbody radiation:

1. Straight line approximation of blackbody radiation

By observing Figure 4.12, measurement results related to blackbody radiation can be treated as a straight line for the interested wavelength range: 800~900nm, so the signal processing algorithm was modified by subtract one constant value for the whole measurement wavelength range(800~900nm), the constant value is exactly the first value in the interference fringes as approximation. This modification improved system performance for high temperature cases, as shown in Figure 5.21, the curve is smooth for temperature higher than certain value(it is about 1100°C), when temperature is lower than this value, the curve is not stable, which means that it is not suitable method to subtract blackbody radiation.

Figure5.21. Results from BPDI system for temperature increasing from 73 °C to 1310 °C

Figure5.22 . Results from BPDI system for temperature increasing from 363 °C to 1310 °C
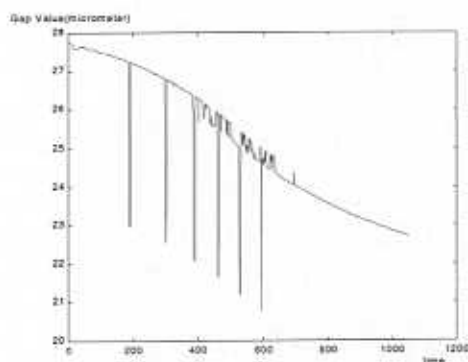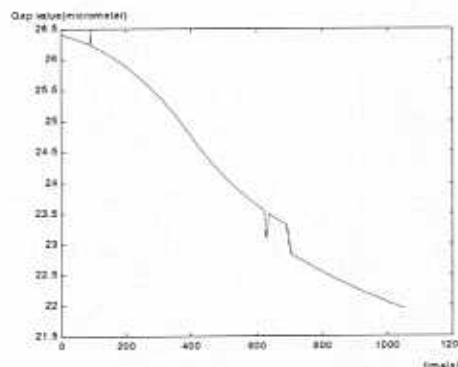
2. Modification to method 1

According to the experimental results from Figure, some modifications to method one is tried: the blackbody radiation will be subtracted only after temperature is over a boundary value, which is selected to be 1100 °C according to experience, before measured temperature reaches this value, no blackbody radiation subtraction at all. The

measurement system performances were improved, while for the temperature values around the boundary value (1100 °C), performance is not stable, as shown in Figure 5.22.

3. Digital filter method

Another problem for method 1 and method 2 is that blackbody radiation can be treated as a general constant for interested wavelength only when temperature is below certain values, see Figure 4.11 and Figure 4.12, for higher temperature, say above 1400 °C , the blackbody radiation curve will tilt up, intensity will not be general constant any more for the measured radiation wavelength range. Thus the above two methods can hardly be applied to proposed temperature measurement range(upto 1600 °C), a new method are proposed and tested.

By modulating LED output light, and combining with digital signal filter (IIR filter, Infinite-Impulse Response filter), background from blackbody radiation can be reduced, especially in high temperature circumstance. When the LED output light is modulated, blackbody radiation is only a DC component in detected signals from spectrometer, it can be filtered out with a high-frequency band pass filter. Within the limit of scanning rate of spectrometer, which corresponds to signal sampling frequency (about 10Hz), the frequency used for LED modulation is selected to be less than 5Hz. The designed filter is shown in Figure 5.23, the pass band is from 2Hz to 5Hz. 3Hz modulation frequency is used to modulate LED output light.
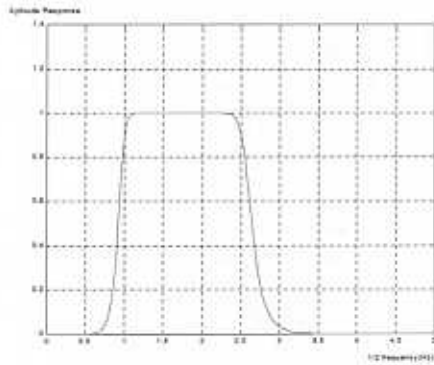
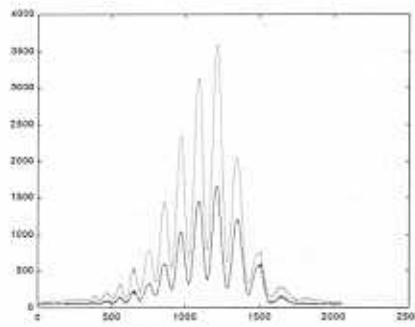**Figure5.23.** Amplitude response of IIR filter.

Figure 5.24. Interferogram results. The lower curve shows signal after filter, the higher curve line is original signal with blackbody radiation.

5.3.4 Experimental results after blackbody radiation reduction

After digital signal processing on the modulated light signal, inteferograms are shown in Figure 5.24, blackbody radiation is greatly reduced. This method is applied to measure the whole proposed temperature range (from room temperature up to 1600°C). Typical output light signals are shown in Figure 5.25. Even with different blackbody radiation background at different temperatures, obviously blackbody radiation is reduced, which make the measurement temperature can be upto 1600 °C or even higher. Figure 5.26 shows a gap values vs. temperature curve, which indicate the one-to-one relation between gap value and real time temperature.
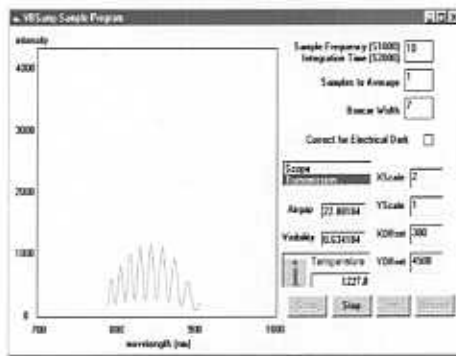
(a) at 1227.0°C
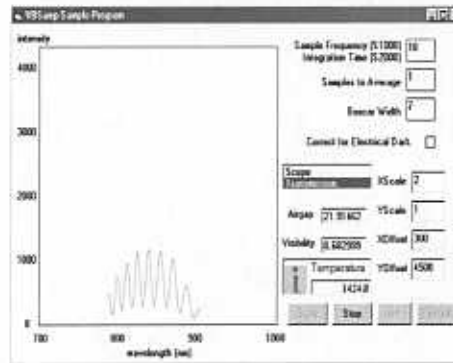
(b) at 1424.0°C

(c) at 1506.0°C

(d) at 1601.0°C

Figure 5.25. Typical output light signals at different temperature

Figure 5.26. Gap values Vs. temperature curve

Figure 5.27 shows calibration curve for a sapphire disk (0.98inch diameter and 0.13inch thickness). The data was obtained every $50\,^{\circ}C$ for the range from $300\,^{\circ}C$ to $1500^{\circ}C$. A $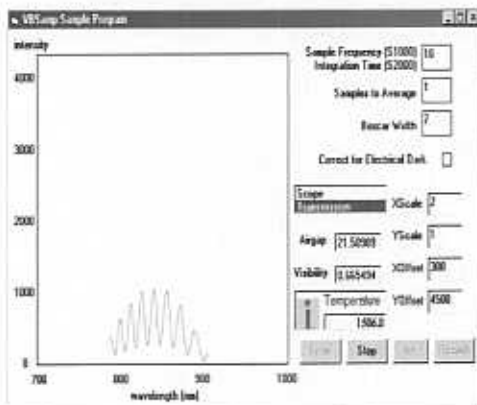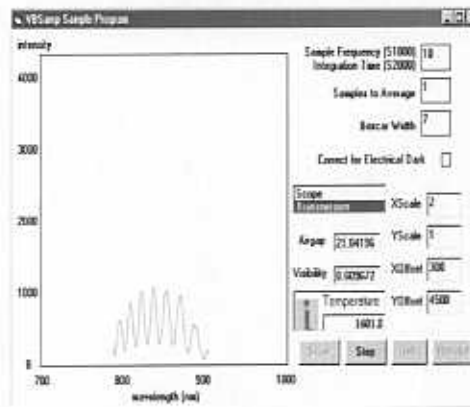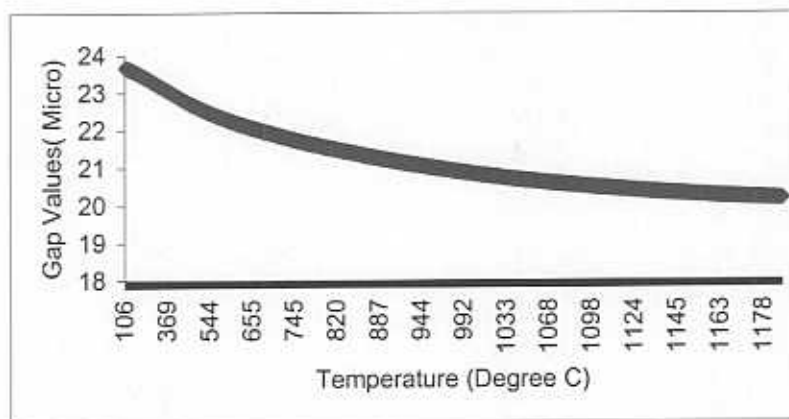4^{th}$ order polynomial was used to do curve fitting instead of the one-order linear equation. The polynomial equation is shown in the upper figure, and the figure below shows the temperature deviation from the curve-fitting results and the experimental measurement results of calibration process. The measurement with the same sapphire disk was repeated three times as shown in Figure 5.28. The good repeatability between the temperature and gap values is achieved. To determine the performance for these three different measurement processes, each of these curves are evaluated separately by a calibrated polynomial equation obtained as in Figure 5.27. Figure 5.29. shows the relationship between the thermocouple measured temperature and the sapphire sensing system output temperature after calibration. The ideal curve will be a straight line crossing the origin with a slope value of 1, assuming the sapphire sensing system output is equal to the thermocouple output. As shown in the figure, the calibrated line is very close to the ideal straight line, which means that the accuracy of the designed sapphire sensing system is at least comparable to B-type thermal couple. The temperature deviation of each curve from the calibrated results is shown in Figure 5.30, which indicates that all of these three measurements have errors in the range of $\pm 4\,^{\circ}C$ (accuracy 0.26% for $1500\,^{\circ}C$) for a temperature range higher than $300\,^{\circ}C$, assuming type B thermocouple measurement results are absolutely accurate and the curve-fitting equation is exactly right. For temperatures lower than $300\,^{\circ}C$, one temperature curve shows errors of about $12\,^{\circ}C$.

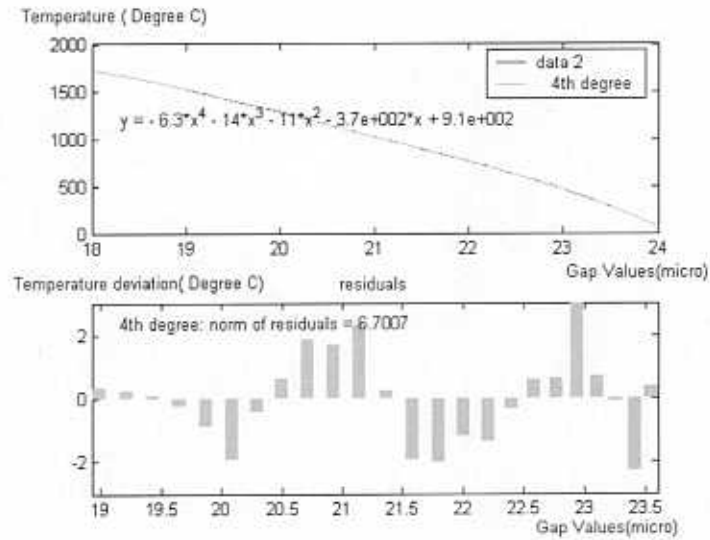Figure 5.27. Curve-fitting for calibrated data for sapphire disk with thickness 0.13inch.
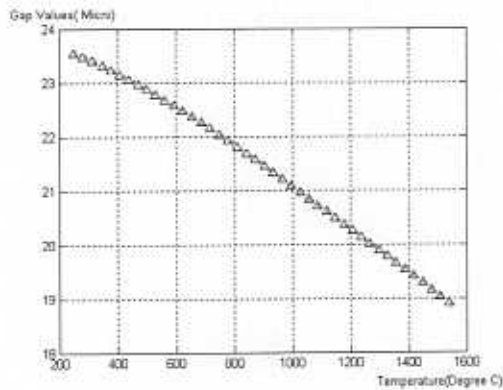
Figure 5.28. Relationship between temperature and gap values measured three times with a sapphire disk with thickness 0.13inch. The three different processes are represented by $\bullet, \Delta, and +$ respectively.
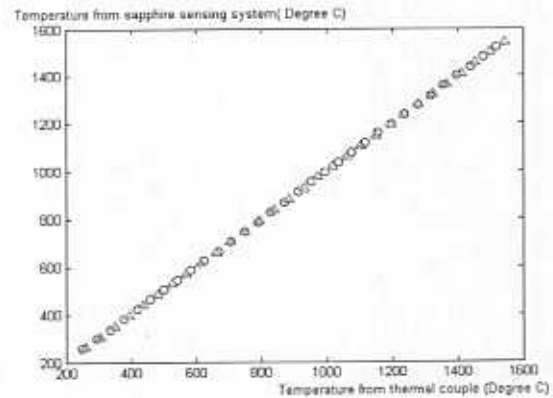
Figure 5.29. Relationship between thermal couple measured temperature and sapphire sensing system output temperature.
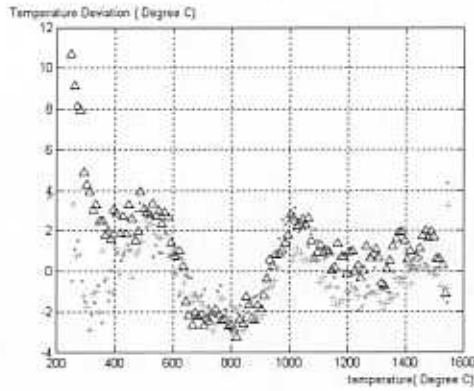
Figure 5.30. Temperature deviation evaluation for each curve in Figure 5.28 with calibrated equation from Figure 5.27. Three different process represented by $\bullet, \Delta, and +$ respectively.
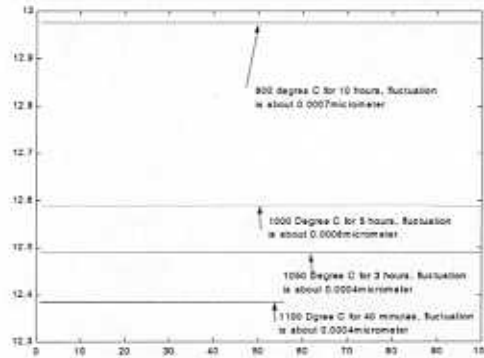
Figure 5.31. Sensing system stability were tested at different temperatures.

According to Equation (4.15), the resolution for this sensor depends on the selected thickness of the sapphire disk, the thicker the disk is, the higher resolution it can achieve. As the thickness increases, the interference fringes will become dense, which will be limited by the resolution of commercially available OSA. For the sapphire disk used in the above three measurements, the whole measurement range 225°C ~1580°C, the gap changed from 23.58 to18.84 micrometer. The average gap change is thus 0.0035micrometer/ °C. The spectrometer has a resolution of 0.002 micrometer on spectrum measurement, which means that the resolution is less than 1 °C for the designed temperature measurement system, the measurement results are at least comparable to the B type thermocouple used for temperature monitoring.

System performance stabilities were tested continuously for different temperature values, results are shown in Figure 5.31. According to the marked gap value fluctuations, the temperature fluctuations are all within $1^\circ C$ after calibration.

5.4. Further experimental results on BPDI system

5.4.1 Precise measurements

Precise measurements were performed to characterize the reproducibility of the measurements by the BPDI optical temperature measurement system. Four experiments were conducted to determine the repeatability of the temperature measurements. Fig. 5.32 provides the results of the temperature measurements repeated seven times up to $1600^\circ C$. Fig. 5.32 (a) demonstrates the exceptional repeatability of the temperature measurements, and Fig. 5.32 (b) shows the deviation of the measurement results from the BPDI sensor system with those of the B type thermocouple, which was used as the temperature reference. For temperature over $1000^\circ C$, an accuracy of $\pm 4^\circ C$ relative to the B type thermocouple was achieved for repeated temperature measurements, which represents 0.25% of the full measurement scale.

5.4.2 Longterm stability tests

In industrial field environments, sensor performance parameters such as reduced requirements on accurate optical alignment, insensitivity to vibrations, and ease of installation , which are generally required by most applications, can not be easily met by current optical sensors. The BPDI optical temperature measurement system design takes advantages of both optical fibers and bulk optics to meet those requirements for field applications. Bulk optics is convenient for reducing the required tolerances on optical alignment and also for reducing the senstivitty to vibration. The optical fiber can transmit light for a long distance with small attenuation and is easily implemented in industrial environments because of its small size, light weight and immunity to electromagnetic interference (EMI).

(a)   (b)
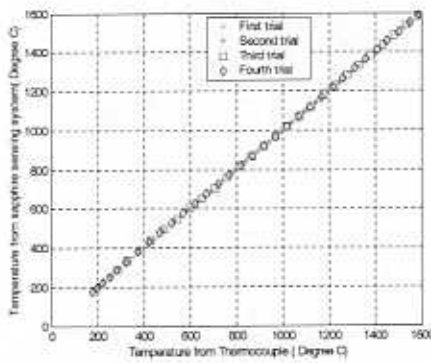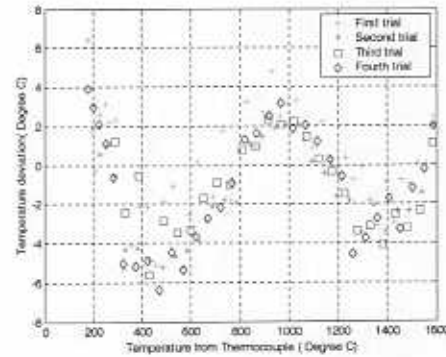
Figure 5.32: (a) BPDI sensor temperature measurement versus thermocouple temperature measurement

(b) Deviation of BPDI temperature from thermocouple temperature

The results of the long term stability tests are shown in Fig. 5.33. These experiments were carried out for different temperature environments. The results for room temperature stability testing are shown in Fig. 5.33a, and the results for 300°C in Fig. 5.33b. As shown in this figure, the long-term performance of the BPDI optical temperature

measurement system is comparable to the thermocouple performance. Fig. 5.33 (c) shows the temperature differences between the thermocouple and the BPDI system for a time duration of over 150 hours. The results show the maximum deviation is in the range of $\pm 2\,°C$. Fig. 5.33 (d) shows the performance degradation of thermocouple for a long term run at $1200\,°C$, while optical thermometer performs well because of the optical materials survivability.
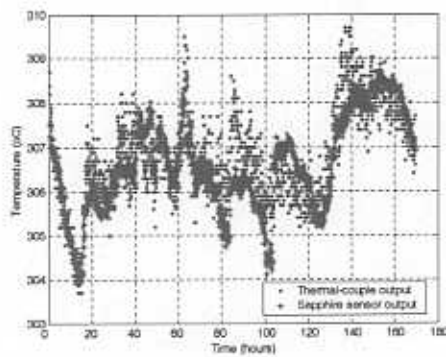
(a) At 306°C
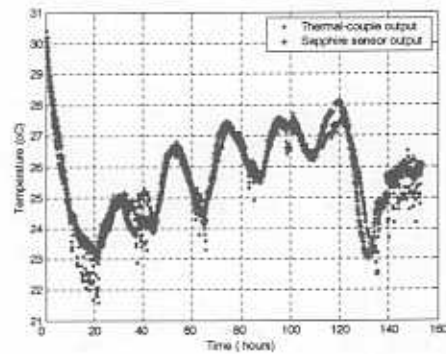
(b) At 26 °C
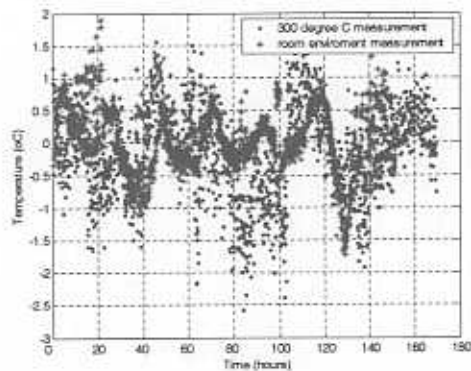
(c) Temperature deviation between thermocouple and optical thermometer
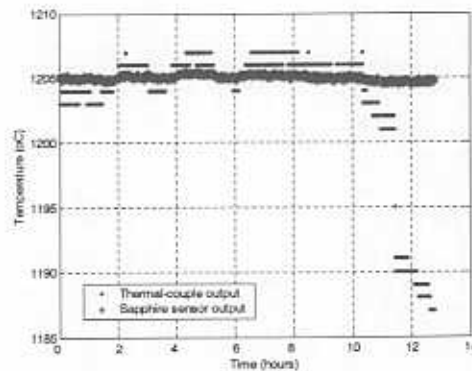
(d) At 1205 °C

Figure 5.33: Long term stability test results

5.4.3 Sensitivity tests

Interferometric sensors have extremely high sensitivity by detecting the differential phase change of an optical signal. The BPDI system provides resolution better than 0.1°C for a wide dynamic measurement range, which is an advantage over other traditional thermometers, such as thermocouple and optical pyrometers.

In general, the resolution of the sensor system is usually interpreted by the standard deviation of a series of temperature measurements at a constant temperature. It is common to use twice the standard deviation as the direct measure of resolution. The evaluation of the sensor resolution was performed using a calibrated sensor at room temperature and also at 618°C. In the test, 1000 temperature values were acquired continuously and the resulting histogram is plotted in Fig. 5.34. The standard deviation of the temperature data was calculated to be $\sigma=0.0348$°C and $\sigma=0.0343$°C, respectively. Therefore, the resolution of the sensor system was estimated to be $2\sigma=0.0696$°C and $2\sigma=0.0686$°C. The normalized resolution with respect to the dynamic range of the system was 0.005% of the full scale. Further improvement can be achieved by increasing the resolution for the spectrograph measurement and signal processing algorithm for phase shift recovery in the interferometer.

(a)   Room temperature

(b) At618.5°C
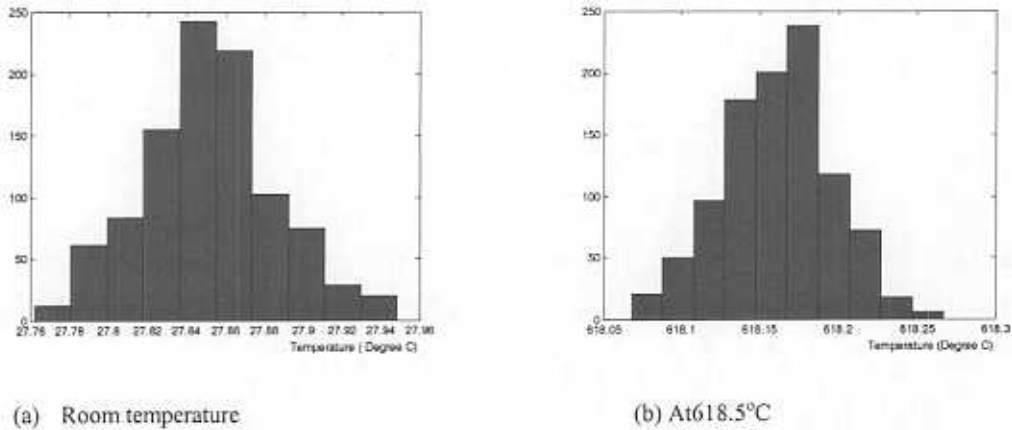
Figure 5.34: Histogram of temperature measurement

5.4.4 Self-calibration capability tests

The BPDI technology extracts temperature information by absolute measurement of the phase shift of orthogonally polarized light, which is attractive for harsh environment applications because of no requiring of initialization and/or calibration when the power is switched on. To make the absolute measurement meaningful, a self-compensating capability is desired so that the optical power fluctuations and fiber loss changes can be fully compensated.

By self-referencing the two orthogonal polarized lights, the BPDI technology posses a self-compensating capability. To evaluate the self-compensating capability of this optical temperature measurement system, the output temperature variations are monitored when the optical source power is changed by changing its driving current. Fig. 5.35(a) shows the output temperature variations as a function of the normalized optical power of the optical source (LED), as shown, temperature variation range is limited to ±0.45°C for

total optical power changes up to 90%. Theoretically speaking, changing the driving current of a semiconductor optical source (LED) would also change the spectrum in addition to the optical power level change, the distortion of the source spectrum would also introduce error to the measurement results through the non-centered filtering effect. Therefore, the measurement results shown in Fig. 5.35(a) also indicate the contribution from the source spectrum distortion. To evaluate the self-compensating capability of this optical temperature measurement system, the output temperature variations are monitored when the multimode fiber was bent to change the fiber attenuation. Fig.5.35 (b) shows the temperature variation is in the range of ±0.4°C for fiber attenuation up to 9dB.
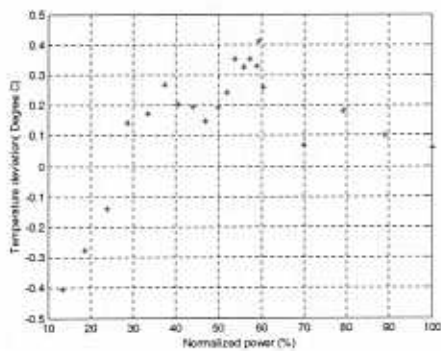
(a)BPDI System measured temperature variations as a function of the normalized optical power
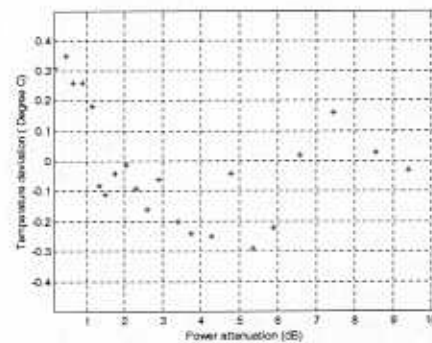
(b)BPDI system measured temperature variations as a function of fiber losses

Figure 5.35: self-calibration capability tests

Chapter 6. Conclusions and Future work

This chapter will summarize the current status on the proposed research and highlight the future work needed to complete the dissertation work. The descriptions will include the work on the design and optimization of the sensing system on both hardware and software, full evaluation of the optical sensing system, the sensor prototype fabrication and implementation, and the practical application.

In this report, based on the two types of sensing elements and three detecting mechanisms, three different temperature-sensing schemes were investigated to determine an optimal approach for high temperature measurement in coal gasification systems. Based on evaluations to date and analysis of the experimental results, the broadband polarimetric differential interferometry (BPDI) was chosen for further prototype instrumentation development. This approach is based on the self-calibrating measurement of the optical path length changes in a single-crystal sapphire disk, which is a function of both the temperature dependent birefringence and the temperature dependent dimensional changes. Future work will focus on this broadband polarimetric differential interferometry (BPDI) sensor technology, full evaluation of its performance, mainly measurement repeatability, measurement resolution, long-term run system stability and self-calibration capability and etc; further optimization of the system design and fabrication of a prototype for a full field demonstration at Global Energy Technology's Wabash River Facility. The sensor instrumentation will be designed for continuous

operation in an actual slagging coal gasifier which operates under high temperatures and extremely corrosive conditions.

6.1 Evaluation of the system performance

The BPDI system was designed and initially demonstrated to be capable of measure temperature up to 1600 °C. This approach is based on the self-calibrating measurement of the optical path length differences in a single-crystal sapphire disk, which is a function of both the temperature dependent birefringence and the temperature dependent dimensional changes. Those experimental results demonstrate the technical feasibility of the sensor technology, a complete and systematic performance evaluation of this sensor will be performed. These test results will also serve as feedback information to further improve the system design. The preliminary test tasks will include:

1. **Reproducibility Testing**

Precise measurements were performed to characterize the reproducibility of the measurements by the BPDI optical temperature measurement system. Additional experiments will be conducted by applying to a certain preset point repeatedly from one direction (increasing or decreasing), the largest difference of the sensor output can be used to specify the repeatability of the sensor.

2. **System stability test**

In industry, high accuracy and low maintenance cost thermometers, which implies long life and stability of calibration, are highly desired, especially in harsh environments where temperature measurement technologies are difficult to apply. System drift needs to be characterized in both short term and long term drift for this system. Short term drift will be characterized to specify the warming-up time of the system in order to obtain a reasonable stable reading. By keeping the sensor head at certain temperatures for a relatively longer time duration, The long-term drift, i.e the deviation of temperature readout from the designed optical temperature measurement system compared with thermocouple readouts will be evaluated.

3.   Resolution evaluation

Resolution of the system is the minimum change of the temperature value necessary to produce a detectable change at the output of the designed system. The standard deviation is a very good measure of the resolution of the temperature sensors. The standard deviation of the sensor can be measured after the temperature sensors are calibrated.

4. Self-calibration capability tests

The BPDI technology extracts temperature information by absolute measurement of the phase shift of orthogonally polarized light, which is attractive for harsh environment applications because of the lack of initialization and/or calibration when the power is switched on. To make the absolute measurement meaningful, a self-compensating capability is desired so that the optical power fluctuations and fiber loss changes can be fully compensated The self-calibration capability of the system will be tested by both

bending the fiber to introduce power losses to the system and reducing the driving current to reduce LED input power and spectrum distribution.

6.2 Optimization of the system design

Based on the BPDI technology and results of laboratory tests and calibrations, design on both hardware and software for signal processing will be optimized to improve the performance. A complete prototype sensor instrumentation system will be designed and implemented for reliable and accurate high temperature measurement.

First, resolutions of the system depend both on the thickness of sapphire sensing element and the resolution of optical spectrum analyzer. Further tests will be done to find the optimal resolution.

Second, to simplify the signal detecting unit structure, new modulation methods on optical source will be tried to reduce blackbody radiation. Thus, the algorithm used to do the signal demodulation and gap value calculation in computer will be optimized.

Third, the software design will be upgraded for the whole system. By employing Visual_BASic or LabVIEW; a graphical user interface (GUI) will be used to display the data for inspection and the data will also be stored on hard disk for further analysis.

6.3 Design and fabrication a field ready prototype sensor system

A sensing tube prototype, which contains the sensing element and optical reflector, is needed to survive high temperature upto 1600^0C when the sensing head is placed physically in the coal gasifier. A single crystal sapphire tube is employed to protect and hold sapphire sensing elements and right angle zerconia prism, which works as an optical reflector. Combining sensing head and polarizer/analyzer with fiber collimator to a whole entity improves mechanical stability. The final version for this sensing head structure is simple and cost-effective for high temperature sensing, and robust enough to survive in real engineering environments. The following tasks are needed:

Task 1. Define requirements – in conjunction with our industrial collaborator, the requirements for the system and system integration with the existing gasification facility will be outlined.

Task 2. Design and fabricate a ruggedized sensor system – based upon the requirements generated in the preceding task, the field test ready prototype system will be designed and fabricated.

Task 3. Design and fabricate a protective housing – although the corrosion resistance of the single crystal sapphire material has been documented in laboratory testing, special consideration will be given to the required mechanical protection of both the sensor probe and the associated signal demodulation system.

Task 4. Laboratory test out and calibration – prior to the actual installation of the temperature sensor system in the gasification unit, the entire system will be tested in the laboratory to ensure proper operation.

6.4 Field test

For field test, consideration of the required environmental performance in a slagging gasifier was a prime concern in the design of the optical sensor components, which must physically reside in the gasification unit. According to the properties of the selected materials for sensing head fabrication, it has potential to survive the high temperature harsh environments. High-density polycrystalline aluminum oxide and transformation-toughened zirconium oxide were found to provide the best corrosion resistance out of a very wide range of oxide and non-oxide materials tested. Because of their corrosion resistance, single crystal sapphire and fully stabilized cubic zirconia were chosen as the preferred optical materials for fabrication of the temperature sensor probe assembly. Working closely with our partner in this project, Global Energy Technology's Wabash River Facility, coal slag samples were obtained. Results of the slag immersion testing indicate that the single crystal sapphire exhibits even better performance than the polycrystalline alumina (as would be expected by elimination of the grain boundary regions).

The sensor instrumentation will be designed for continuous operation in an actual coal gasification facility under high temperatures and extremely corrosive conditions. The field test will be run for multiple months to be able to reliably demonstrate the capability of the operation in the extremely harsh gasification environment. Before the designed sensing system is installed in the coal gasifier, requirements for temperature of operation position in the gasifier, stages to be instrumented in the gasifier, slagging conditions at the temperature measurement points, length into hot zone, length of refractory, location of electronics, etc. will be specified by our partner, Global Energy Technology, Inc.

Future tests and evaluations of the sensing system at Wabash Gasification facility will be the following:

Task 1. Installation of the sensor probe head components into gasification unit – a "dummy" probe will be installed in the gasification unit to determine performance of the components in an operating slagging gasifier.

Task 2. Site preparation and installation – the field test site will be prepared for installation of the sensor system. After all external infrastructure is installed for communication of the signal to appropriate location, the sensor probe will be installed in the gasfier.

Task 3. Testing and data collection – the system will be operated for several months to evaluate the performance.

Task 4. Data analysis - the data obtained during the field test will be analyzed to determine the performance of the temperature sensor in the gasification unit.

Reference

1. N. Berkowitz. "Coal gasification, a "state-of-the-art" review." Edmonton, Alberta Research, 1973.

2. Schilling, Hans-Dieter. "Coal gasification: existing processes and new developments". [2nd rev. ed.], H-D. Schilling, B. Bonn, U. Krauss, London : Graham & Trotman, 1981.

3. Hoffman, E. J. (Edward Jack), "Coal gasifiers". Laramie, Wyo. Energon Co., 1981.

4. Hastie, E.plante and D.Bonnell, " Alkali Vapor Transport in Coal Conversion and coal combustion systems", ACS Symposium Series, vol. 179 Metal bonding and interactions in high temperature systems with emphasis on alkali metals(1982)

5. T.Sun. "Alkali corrosion of ceramic materials", Ceramic News, 2(4)1-2, 1991

6. J.Schlichting, "Oxidation and hot corrosion behavior of SiN and SiAlON". Pp.627-632 in Nitrogen ceramics. Edited by F.L.Riley. Noordhoff, Leyden, 1977

7. J.Smialik and N.Jacobson, "Mechanism of strength degradation for hot corrosion of alpha-SiC," J.Am. Ceram.Soc., 59(10)741-752, 1986

8. M.Feber,J.Ogle,V.Tennery and T.Henson. "Characterization of corrosion mechanisms occurring in a sintered SiC exposed to basic coal slags," J.Am.Ceram.Soc. 68(4) 191-197,1985

9. Matthias Ralf Werner, and Wolfgang R. Fahrner, "Review on Materials, Microsensors, Systems, and Devices for High-Temperature and Harsh-Environment

Applications". IEEE transactions on industrial electronics, vol. 48, no. 2, april 2001, pp249-257

10. J.R.Leigh. Temperature Measurement and Control, Chapter 5, Perter Peregrinus Ltd, London, United Kingdom, 1988

11. Lu, G. Bheemul, H.C. Yan, Y. "Concurrent measurements of temperature and soot concentration of pulverized coal flames". Instrumentation and Measurement Technology Conference, 2001. IMTC 2001. Proceedings of the 18th IEEE, pp: 1221 - 1226 vol.2

12. Jesus Castrellon, Gonzalo Paez,Marija Strojnik , "Radiometric analysis of a fiber optic temperature sensor". Optical Engineering, Vol. 41 No. 6, June 2002. pp 1255-1261

13. K.M.Koo, J.H.Kim.S.B.Kim, H.D.Kim, D.Y.Ko, " Ultrasonis thermometry system for measuring very high temperatures using high resolution signal processing". Proceeding of the IECIC 2001, Aug 2001.pp 229-232

14. M.Feber and V.Tennery. " Behavior of Tubular ceramic heat exchanger materials in Acidic ash from coal-oil-mixture combustion." Ceram.Bull, 62(2) 236-243, 1983

15. D.Mckee and D.Chatterji, "Corrosion of silicon carbide in gases and alkaline melts," J. Am, Ceram, soc 59(9-10)441-444, 1976

16. T. Sun, " Alkali corrosion of coal gasifier linings," master's thesis Virginia Polytechnic Institute, 1986

17. M.Van roode and J. Price, " Corrosion resistant coatings for ceramic heat exchanger tubes operating in highly corrosive environments." Pp 625-633 in high performance ceramic coatings and films, published by Elsevier Science Publishers, 1991

18. G.R. Pickrell, "High Temperature Alkali Corrosion of Low Expansion Ceramics", Ph.D. Dissertation, Virginia Tech, 1994

19. Ernest Magison, "Temperature measurement-Physical principles underlie the four common methods.", Industrial temperature measurement, November 2001,pp39-41

20. Temperature and humidity measurement, editor Robin E. Bentley, handbook of temperature measurement, Vol1, Singapore ; New York : Springer, 1998

21. L.C. Lynnworthand E.H.Carnavale. Ultrasonic thermometry using pulse techniques. In H.H.Plumb, editor, Temperature: its measurement and control in science and industry, vol 4, pp 715-732. Inst.Soc. Ameica, Pittsburgh, 1972.

22. S.F.Green. Acoustic temperature and velocity measurement in combustion gases. In 8th Int. Heat Transfer Conf., San Francisco, August 1986/

23. Selected topics in advanced solid state and fiber optic sensors. Edit by S.M. Vaezi-Nejad. Publishe by the institute of Electrical Engineers, London, United Kingdom. 2000, IEE circuits, devices and systems series 11.

24. D.P.Dewitt and G.D.Nutter, editors. Theory and practice of radiation thermometry. John Wiley&Sons, Inc. New York, 1988.

25. R.O.Claus, M.F. Gunther, A. Wang, K.A.Murphy, " Exitrinsic Fabry-Perot sensor for strain and crack opening displacement measurement from –200 to 900 °C", Smart Materials and structures, Vol1, no.3, 1992

26. M.Sun. Fiberoptic thermometry based on photoluminescent decay times. In J.F.Schooley, editor. Temperature: its measurement and control in science and industry, vol 6, pp 715-719. Amer. Inst.Phys, New York, 1992.

27. Z.Zhang, K.T.V.Grattan, and A.W.Palmer. Fiber-optic high temperature sensor based on the fluorescence lifetime of alexandrite. Rev.Sci.Instrum.63: 3869-73, 1992

28. B.W.Noel,W.D.Turley,W.Lewis,K.W.Tobin, and D.L.Beshears.Phosphor thermometry on turbine-engine blades and vanes. In J.F.Schooley, editor. Temperature: its measurement and control in science and industry, vol 6, pp 1249-54. Amer. Inst.Phys, New York, 1992.

29. O.Iida, T.Iwamura,K.hashiba, and Y.Kurosawa. A fiber optic distributed temperature sensor for high-temperature measurements. In J.F.Schooley, editor. Temperature: its measurement and control in science and industry, vol 6, pp 745-749. Amer. Inst.Phys, New York, 1992.

30. H. Xiao, J. Deng, R. May, and A. Wang, "Single crystal sapphire fiber-based sensors for high-temperature applications," SPIE Conference on Harsh Environment Sensors II, Bonston, MA, September 19 (1999).

31. Yibing Zhang , Qi. Bing, et. al. "Single-crystal sapphire high-temperature sensor" Proc. SPIE Vol. 4578, p. 191-197, Fiber Optic Sensor Technology and Applications 2001

32. C. P. Khattak and F. Schmid, "Growth of Large-Diameter Crystals by HEM for Optical and Laser Applications," *Proc. SPJE, 505,* 4-8 (1984).

33. C. P. Khattak, A. N. Scoville and F. Schmid, "Recent Developments in Sapphire Growth by Heat Exchanger Method (HEM)," *Proc. SPJE,* 683, 32-35 (1986).

34. F. Schsnid and C. P. Khattak, "Current Status of Sapphire Technology for Window and Dome Applications." *Proc. SPIE,* 1112. 25-30 (1989).

35. F. Schmid, M. B. Smith and C. P. Khattak, "Current Status of Sapphire Dome Production," *Proc. SPIES*, 2286, 2-15 (1994).

36. C. P. Khattak, F. Schmid and M. B. Smith, "Correlation of Sapphire Quality with Uniformity and Optical Properties." *Proc. SPIES*, 3060, 250-257 (1997).

37. H. E. LaBelle, "EFG the Invention and Application to Sapphire Growth,". *Crystal Growth*, 50, 8-17 (1980).

38. H. E. LaBelle, J. Serafina and J. J. Fitzgibbon, "Recent Developments in Growth of Shaped Sapphire Crystals," *Proc. SPIES*, 683, 36-40 (1986).

39. J. W. Locher, H. E. Bennett, C. P. Archibald and C. T. Newmyer, "Large Diameter Sapphire Dome: Fabrication and Characterization," *Proc. SPIES*, 1326, 2-10 (1990).

40. J. W. Locher, H. E. Bates, W. C. Severn, B. G. Pazol and A. C. DeFranzo, "80-mm-EFG Sapphire Dome Blanks Yield High Quality, Low Cost Single Crystal Domes," *Proc. SPIES*, 1760, 48-54 (1992).

41. V. N. Kurlov and S. N. Rossolenko, "Growth of Shaped Sapphire Crystals Using Automated Weight Control," *J. Crystal Growth*, 173, 417-426 (1997).

42. D.C. Harris. Materials for infrared windows and domes, SPIE Press, Bellingham WA, 1999

43. "Handbook of optics-fundamentals, techniques& design". Michael Bass chief editor.(second edition) Volum II. Sponsored by the OSA. McGraw-Hill, 1995.

44. J.B. Wachtman, Jr. and L.H. Maxwell.'Strength of synthetic single crystal sapphire and ruby as a function of temperature and orientation. J. Am. Ceram, Soc. 42, 432-433, 1959

45. R.L.Gentilman, E. A. Maguire, H.S. Starrett, T.M. Hartnett and H.P. Kirchner. " strength and transmittance of sapphire and strengthened sapphire" J.Am.Ceram. Soc, 64, c116-c117 , 1981

46. J. W. Fischer, W.R.Compton, N.A. Jaeger and D.C. Harris. " strength of sapphire as a function of temperature and crysta orientation.' Proc. SPIE. 1326, 11-22, 1990

47. D.C. Haris and L.F. Johnson, " Navy mechanical test results from the sapphire statistical chand RR program, Proc, SPIE 3705, 44-50, 1999

48. D.C. Harris, " Overview of progress in strengthening sapphire at elevsated temperature, proc, SPIE 3705, 2-11, 1999

49. Frederick Schmid, Keil A. Schmid, Chandra P. Khattak, Peter Duggan. 'Increase of the strength of sapphire by heat treatments". SPIE 3705, 36-43, 1999

50. Frederick Schmid, Chandra P. Khattak, Keil A. Schmid, Svetlana G. Ivanova. 'Increase of high temperature strength of sapphire by polishing, heat treatments and doping". SPIE 4102, 43-51, 2000

51. M.R. Borden and J.Askinazi, "Improving sapphire window strength." Proc. SPIE,3060,246-249, 1997

52. A. Dandridge and A. D. Kersey, "Overview of Mach-Zehnder sensor technology and applications", Proceedings of SPIE 985, Fiber Optic and Laser Sensors VI, Boston, Sept. 1988.

53. A. Wang, S. Gollapudi, R. G. May, K. A. Murphy, and R. O. Claus, "Sapphire optical fiber-based interferometer for high temperature environmental applications," J. of Smart Materials and Structures, 4, 147-151 (1995).

54. A. Wang, S. Gollapudi, K. A. Murphy, R. G. May, and R. O. Claus, "Sapphire-fiber-based intrinsic Fabry-Perot interferometer" Optics Letters, vol. 17, no. 14, pp.1021-23 (1992).

55. Amnon Yariv, Optical Electronics in Modern Communications(5th), Chapter1. Oxford,1997

56. A. Wang, H. Xiao, J. Wang, Z. Wang, W. Zhao, and R. G. May, "Self-Calibrated Interferometric/Intensity-Based Optical Fiber Sensors," J. of Lightwave Technology, vol. 19, no. 10, 2001 pp1495-1501.

57. John G. Proakis and Dimitris G. Manolakis, *Digital Signal Processing: Third Edition*, Prentice-Hall, 1996.